THE ASTROPHYSICAL JOURNAL, 281: 31–55, 1984 June 1

INFALL OF GALAXIES INTO THE VIRGO CLUSTER AND SOME COSMOLOGICAL CONSTRAINTS

R. BRENT TULLY AND EDWARD. J. SHAYA
Institute for Astronomy, University of Hawaii
Received 1983 February 3; accepted 1983 November 11

ABSTRACT

A family of mass models have been developed to describe the observed infall of galaxies in the Virgo Southern Extension toward the Virgo Cluster. The requirement that the mass models also explain the motion of our Galaxy with respect to the Virgo Cluster provides some constraints of cosmological interest. If the age of the universe is $10 < t_0 < 15$ Gyr, then there is a rough coincidence between the mass required to explain the infall pattern of galaxies near to the cluster, the mass required to explain the motion of our Galaxy, and the mass implied for the central cluster by the virial theorem. In this case, most of the mass of the supercluster must reside in the Virgo Cluster. Since 80% of the light of the supercluster lies at larger radii, the mass-to-light ratio must drop by perhaps an order of magnitude going out from the central cluster. If $t_0 < 10$ Gyr, models can be formulated which require additional mass at large radii, such that there need not be marked variations in M/L with radius. However, it may be difficult to accept that the universe is so young. If $t_0 > 15$ Gyr, there is already *too much* mass at small radii, as implied both by the virial analysis of the cluster and the infall model for the galaxies close to the cluster, to explain the motion of our Galaxy. If it is insisted that the universe is older than this limit, then a tractable conclusion is that the cosmological constant is positive.

With the mass-age models and a census of the distribution of galaxies near the Virgo Cluster, it is possible to estimate the near-future accretion rate of galaxies into the central cluster. The influx of gas-rich systems is sufficiently large that it is plausible that all of the spirals and irregulars presently observed in the Virgo Cluster have arrived on a time scale of a third to half the age of the universe. By contrast, the influx of gas-poor systems is insignificant compared with the number of these kinds of galaxies already in the cluster. There are several indirect indications that the Virgo Cluster was composed mainly of ellipticals and lenticulars until recently, but is in the process of being modified as the consequence of a merger with a large cloud of spiral galaxies.

Subject headings: cosmology — galaxies: clustering — galaxies: formation

I. AN OBSERVATION AND AN IDEA

There is one place within the Local Supercluster where non-Hubble streaming motions are quite evident. In one of the maps of the Virgo II Cloud, or Virgo Southern Extension, that was published by Tully (1982, a variation is produced here as Fig. 1) a pronounced finger can be seen which points toward our position at the origin of the coordinate system. It was recognized that this feature was probably an artifact of the naive prescription that placed galaxies in three-dimensional space in accordance with the assumption of a uniform Hubble flow.

It was already anticipated in that earlier paper that there is a group of galaxies including NGC 4636 and NGC 4665 which, although *blueshifted* with respect to the barycentric velocity of the Virgo Cluster by up to 500 km s^{-1}, is probably located on the *far* side of the cluster. It is predominantly this group which gives rise to the kinematic finger discussed above. If our conjecture about the geometry of the situation is correct, then galaxies in this group have large negative velocities with respect to the Virgo Cluster and will fall into Virgo in much less than a Hubble time. There are enough galaxies in this one group to cause a substantial increment to the number of spiral systems in the Virgo Cluster. This observation prompted the speculation that most, or perhaps all, spirals in Virgo are recent arrivals.

It is well established that galaxy morphology is a function of location, with a far higher rate of occurrence of ellipticals and lenticulars in rich clusters than in the field (Dressler 1980). If, indeed, there is a significant regular influx of *spiral* galaxies into clusters, then unless these newcomers are being converted into early systems, the percentage of gas-rich galaxies in clusters must be on the increase. Ostriker (1980) and van den Bergh (1982) have offered some strong arguments against the notion that spiral galaxies can be transformed into ellipticals. At the time of cluster formation, the segregation between spirals and ellipticals might have been even more extreme than what is observed today.

It occurred to us that *if galaxies were forming at the same time the cluster was forming*, then there might be a combination of mechanisms which would regulate the angular momentum content of the protogalaxies. Nonspherical galaxies that were forming while collapsing toward the cluster core would lose angular momentum due to tidal-locking. Conversely, galaxies formed while expanding away from the cluster would be spun up. The latter mechanism is analogous to the interaction proposed to occur between pairs of protogalaxies (Hoyle 1949; Peebles 1969; Thuan and Gott 1977; Efstathiou and Jones 1979). The galaxies formed during collapse toward the cluster core would be ellipticals and would constitute the first generation cluster members. Spirals formed while expanding away from the cluster, and may or may not be captured later. In addition to this environmental dependence of a torquing mechanism, the tidal field of the supercluster affects the ability of galaxies to accrete new material. Galaxies near the cluster core will be deprived of tenuously held material more effectively than galaxies well away from the cluster.

The rest of this article and the one which follows (Shaya

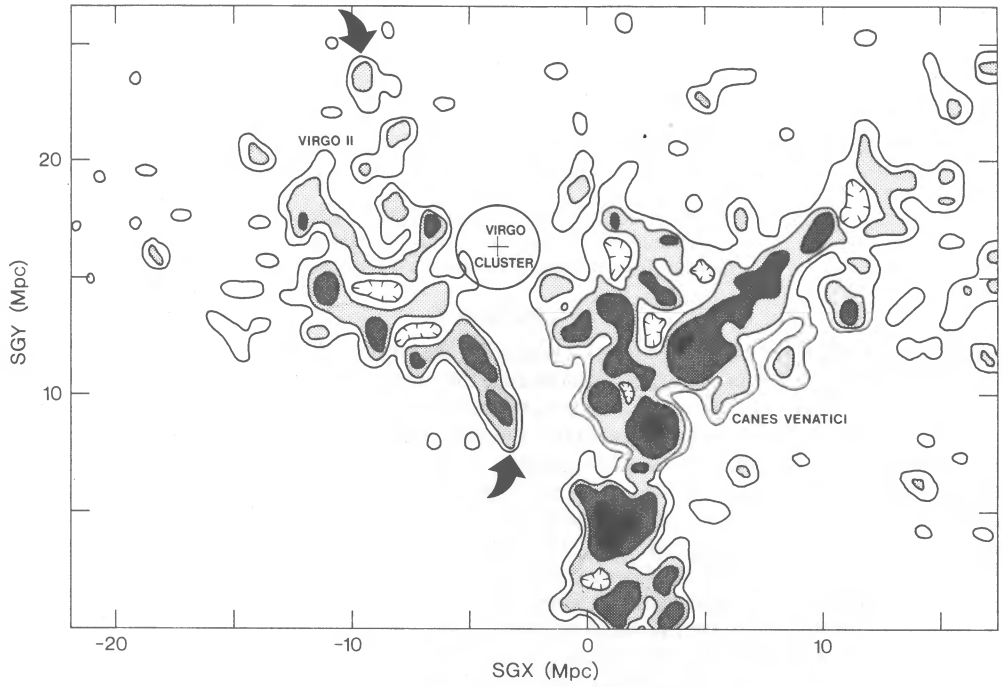

FIG. 1.—A view from the pole of the Local Supercluster of the two principal clouds which constitute the plane of the supercluster. We are located at the origin of the coordinate system. The map was plotted assuming a uniform Hubble flow across the entire region. The elongated NGC 4636/65 feature which points toward us (bracketed by the two arrows) is a kinematic effect caused by the breakdown of the uniform Hubble flow assumption.

and Tully 1984) elaborates on these observational and theoretical issues. In § II, the observed infall of supercluster galaxies into the Virgo Cluster is modeled. The present infall rate is deduced, and we ask how this rate will modify the Virgo population in § IV. The conclusion will be that the spirals found in the Virgo Cluster probably *are* all relatively recent arrivals, so the hypothesis that the first generation members were all ellipticals is worth exploring. The mechanism which might control the angular momentum content of galaxies is discussed in the accompanying article, making use of the tidal field inferred from the Virgo infall model. As an important aside, the fit of an infall model to the observed velocity field of the supercluster provides tantalizing constraints on such important parameters as the age of the universe, variations in mass-to-light with environment, and the cosmological constant Λ. These constraints are discussed in § III. The three appendices provide a résumé of our current understanding of the properties of the 6° Virgo Cluster. A virial analysis of the cluster is included.

II. THE PRESENT INFLUX OF GALAXIES INTO THE VIRGO CLUSTER

a) The Sample

Most of the galaxies outside but near the Virgo Cluster today are found to the south of the cluster. In the discussion of the Local Supercluster by Tully (1982), it was demonstrated that this large-scale structure is composed of only a small number of clouds, with substantial voids in between. It happens that, at the moment, only the Virgo II Cloud is in close proximity to the Virgo Cluster.

As a first step in the analysis, we isolated a region ($92 < \mathrm{SGL} < 117$, $-11 < \mathrm{SGB} < +8$)[1] which generously includes the Virgo Cluster and the proposed infalling group, including about half of the Virgo II Cloud, but which does not extend out to any other major feature in the supercluster. A data set was compiled of all galaxies in the region with measured systemic velocities less than 3000 km s^{-1}. Most of the necessary information was drawn from the Nearby Galaxies Catalog (NBG: Tully and Fisher 1984). The major sources of redshifts for that compendium are the *Second Reference Catalogue* (de Vaucouleurs, de Vaucouleurs, and Corwin 1976), the magnitude-limited Shapley-Ames sample completed by Sandage (1978), and the H I survey by Fisher and Tully (1981). Several very recent sources of redshifts that were not included in the NBG catalog have been added to the present data set (Eastwood and Abell 1978; Peterson 1979; Sulentic 1980). All told, we know of 286 galaxies with $V_0 < 3000$ km s^{-1}, $92 < \mathrm{SGL} < 117$, and $-11 < \mathrm{SGB} < 8$.

The distribution of our sample on the plane of the sky is displayed in three velocity segments in Figure 2. All galaxies with $V_0 < 500$ km s^{-1} are plotted in Figure 2*a*. Systems with $500 \leq V_0 < 1700$ km s^{-1} are plotted in Figure 2*b*. Those with $1700 \leq V_0 < 2600$ km s^{-1} are plotted in Figure 2*c*. There are four galaxies in our sample with $2600 \leq V_0 \leq 3000$ km s^{-1} which are not plotted; all are suspected to be in the background, and none are close to the Virgo core.

These intervals are not chosen haphazardly, of course. The large circle in each frame locates the boundary of the 6° Virgo Cluster (centered on M87 at SGL = 102.9, SGB = −2.3). It can be seen that essentially all low-velocity galaxies in the region under consideration (extending to $V_0 = -624$ km s^{-1}) are located within the 6° core radius. It is this observation which convinced Tammann (1972; also Sandage and Tammann 1976) and, likewise, convinces us that these low-velocity galaxies are all directly associated with the Virgo Cluster (this issue is raised again in Appendix B).

By symmetry with respect to our preferred systemic velocity of 1004 km s^{-1} for the cluster (see Appendix A), the high-

[1] SGL = supergalactic longitude; SGB = supergalactic latitude.

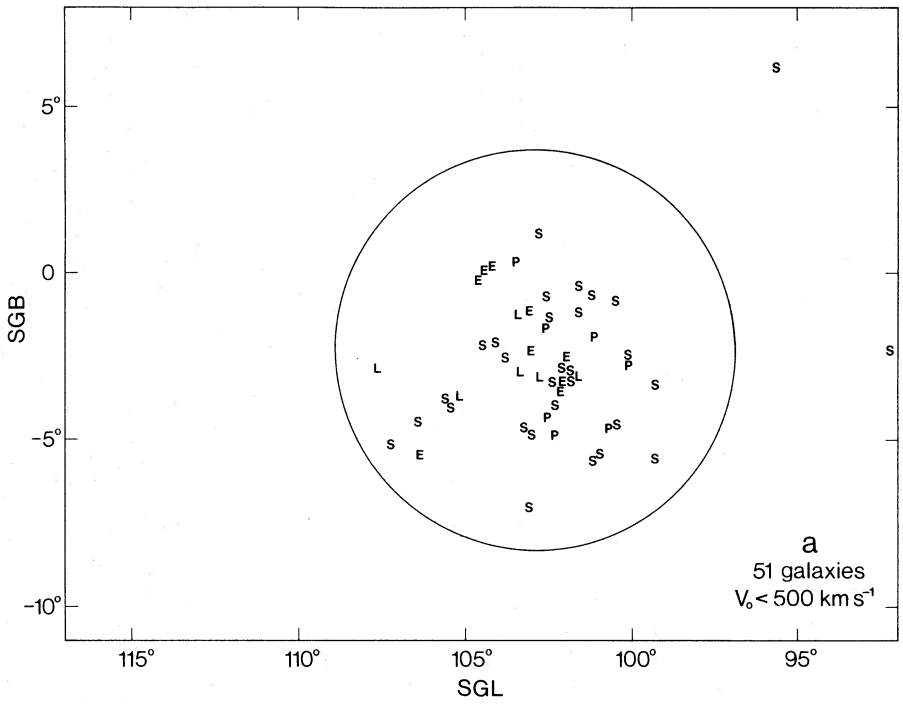

FIG. 2*a*

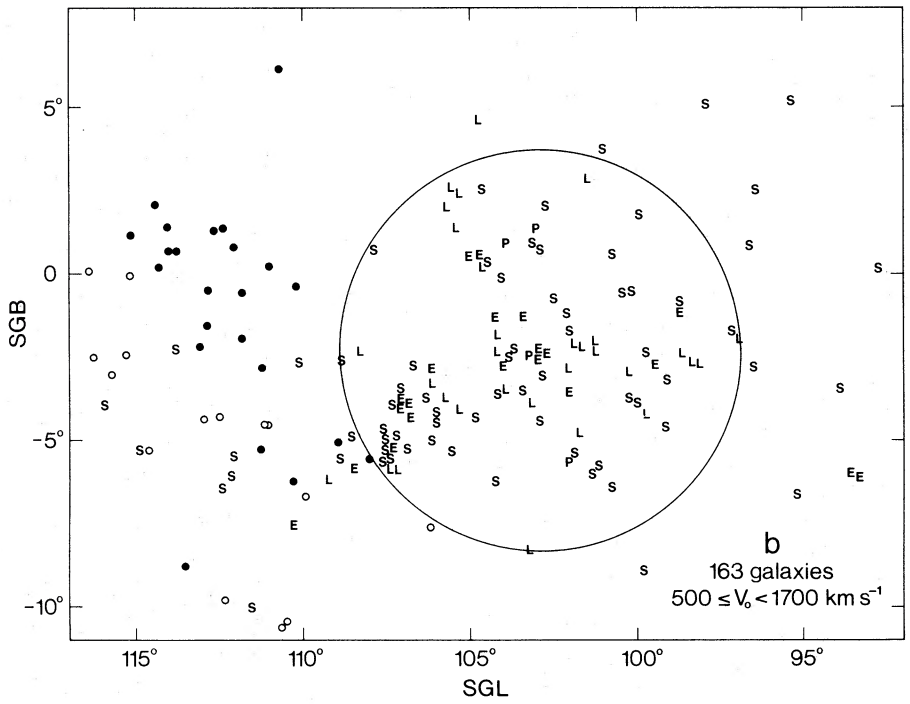

FIG. 2*b*

FIG. 2.—(*a*) Galaxies in the near-Virgo sample with $V_0 < 500$ km s^{-1}. Symbols indicate morphological types: ellipticals (E), lenticulars (L), spirals and irregulars (S), peculiar or unknown (P). (*b*) Galaxies with $500 \leq V_0 < 1700$ km s^{-1}. Filled circles represent galaxies in the Virgo II Cloud which are *blueshifted* with respect to Virgo and are assumed to be beyond the cluster falling in. Open circles represent galaxies in the Virgo II Cloud which are *redshifted* with respect to Virgo and are assumed to lie in front of the cluster falling in. The locations of all other galaxies are indicated by the symbols coded as in Fig. 2*a*.

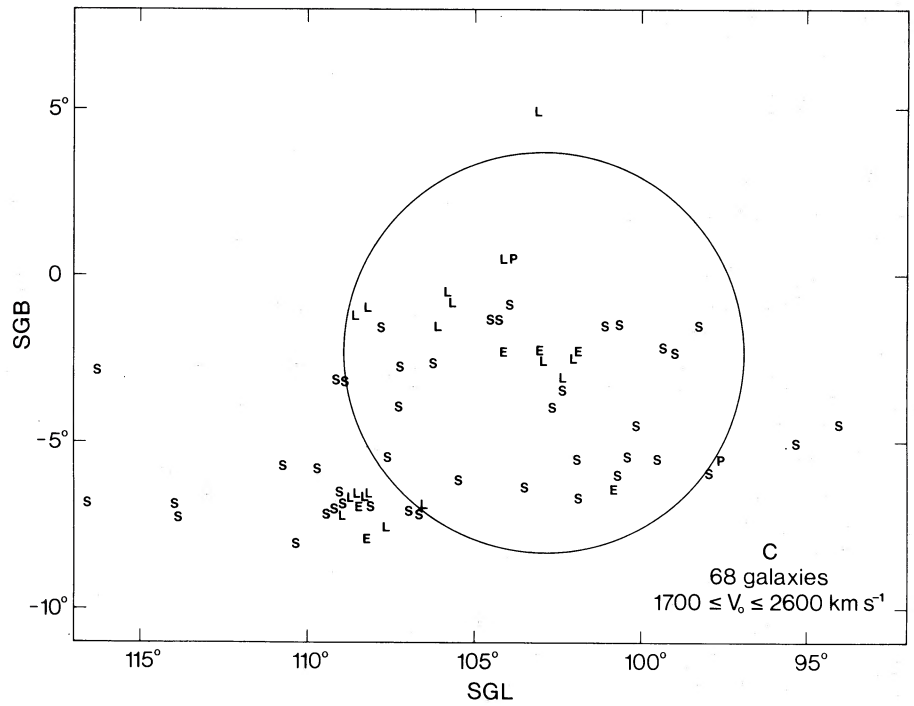

FIG. 2*c*.—Galaxies with $1700 \leq V_0 \leq 2600$ km s^{-1}. The symbol code is the same as in Fig. 2*a*.

velocity tail would be expected to extend out to $+2600$ km s^{-1}. Most of the galaxies plotted in Figure 2*c* once again fall within the 6° radius (the highest velocity is at $V_0 = 2527$ km s^{-1}), with the exception of a substantial clump near SGL = 109°, SGB = −7°. This exception is de Vaucouleurs's (1975) group 46, or Virgo W. Most of the galaxies in this entity, centered in velocity at $V_0 \approx 2200$ km s^{-1}, are early and are small compared with galaxies inside the 6° circle. We have only one H I profile distance estimate to a member of this group, but it gives a distance which is roughly double the Virgo value. Visvanathan and Griersmith (1977) found the mean distance modulus of four galaxies in this group to be 1.9 mag greater than the Virgo modulus. It is concluded that Virgo W is a background group, at about twice the Virgo distance as redshifts would imply. This group may spill over slightly into the 6° circle, but the contamination does not appear to be serious. Otherwise, there is no evidence that foreground-background contamination in the high or low velocity wings of the velocity distribution of the Virgo Cluster is a problem. The 6° radius definition is sufficient to contain essentially all of the extreme-velocity galaxies likely to be associated with the cluster.

The distribution of galaxies in Figure 2*b* is quite different. There are many galaxies with velocities within 700 km s^{-1} of the Virgo Cluster systemic velocity located in the plane of the supercluster with SGL > SGL$_{\rm Virgo}$. This region is part of the Virgo II Cloud. Galaxies which are blueshifted with respect to the systemic velocity of the Virgo Cluster are identified by filled circles in Figure 2*b*, while galaxies which are redshifted are identified by open symbols or the type code. A separation can be seen between the blueshifted and redshifted galaxies. This separation on the plane of the sky makes it clear that spatially distinct structure exists in the region, with random motions which are much less than the range (500–1700 km s^{-1}) observed for the ensemble.

b) Distance to the Virgo Cluster

Our analysis depends on our ability to measure distances to individual galaxies in the field relative to galaxies in the Virgo Cluster. The distance to the cluster can now be determined quite accurately (except for zero point uncertainties) because several precise methods are available and the Virgo sample is quite large.

We rely on four methods to establish the distance scale: the blue magnitude ($M_B^{b,i}$) versus H I profile width (W_{20}^i) correlation (Tully and Fisher 1977):

$$M_B^{b,i} = -5.63 - 5.55 \log W_{20}^i \; ; \qquad (1)$$

the infrared magnitude ($H_{-0.5}^{\rm abs}$) versus H I profile width correlation (Aaronson, Huchra, and Mould 1979):

$$H_{-0.5}^{\rm abs} = 3.60 - 10 \log W_{20}^i \; ; \qquad (2)$$

the Holmberg diameter ($A_{\rm Ho}$) versus H I profile width correlation (Tully and Fisher 1977):

$$\log A_{\rm Ho} = -0.318 + 0.715 \log W_{20}^i \; ; \qquad (3)$$

and the blue-infrared ($B_T^{b,i} - H_{-0.5}$) color-magnitude correlation (Tully, Mould, and Aaronson 1982):

$$H_{-0.5}^{\rm abs} = -17.05 - 2.32(B_T^{b,i} - H_{-0.5}) \, . \qquad (4)$$

These four relationships were derived based on observations of 12 local calibrators in four nearby groups. The Sandage-Tammann (1975) distances to these groups are assumed, but are adjusted to a Hyades modulus of 3.29 mag. For specific information on this sample, see Tully, Mould, and Aaronson (1982). Uncertainties in the zero points of our relationships are of secondary concern for the present discussion. The key question to resolve is whether there is evidence for infall toward Virgo, and to address this question it is only the *relative*

TABLE 1

A. Individual Distance Estimates for Galaxies Inside the 6° Virgo Cluster

							$B-W$		$H-W$		$A-W$		$B-H$			
Name	T	i	$B_T^{b,i}$	$H_{-0.5}$	a_{Ho}	W_{20}^i	$M_B^{b,i}$	D_{BW}	$H_{-0.5}^{abs}$	D_{HW}	A_{Ho}	D_{AW}	$H_{-0.5}^{abs}$	D_{BH}	Meth.	$\bar{D}$
N4178.....	8B	77	11.44	10.14	7.3	294	−19.33	14.2	−21.08	17.5	27.9	13.1	−20.07	11.0	4	14.0 ± 2.7
N4192.....	2X	78	9.91	7.77	11.6	468	−20.45	11.8	−23.10	15.0	39.0	11.5	−22.01	9.1	4	11.8 ± 2.4
N4206.....	4A	78	11.73	10.34	6.6	314	−19.49	17.5	−21.37	22.0	29.3	15.2	−20.27	13.3	4	17.0 ± 3.7
U7279.....	9	85			3.4	249					24.8	25.0			1	25.0
N4216.....	3X	81	10.28	7.33	10.4								−23.89	17.6	1	17.6
N4294.....	6B	70	12.26	10.77	4.3								−20.51	18.0	1	18.0
U7513.....	5	90		10.74	5.0	292			−21.05	22.8	27.8	19.1			2	21.0 ± 2.7
N4388.....	3 P	81	11.17	8.86	8.6								−22.41	17.9	1	17.9
U7547.....	10	50			2.6	112					14.1	18.5			1	18.5
N4450.....	2A	53	10.80	8.06	8.8	363	−19.84	13.4	−22.00	10.3	32.5	12.7	−23.41	19.6	4	14.0 ± 4.0
N4498.....	7B	59		10.76	5.0	222			−19.86	13.3	22.9	15.7			2	14.5 ± 1.7
N4501.....	3A	64	10.05	7.15	9.4	594	−21.03	16.4	−24.14	18.1	46.3	16.9	−23.78	15.3	4	16.7 ± 1.1
N4519.....	7B	48	12.25	10.75	4.2	305	−19.42	21.6	−21.25	25.1	28.8	23.4	−20.53	18.0	4	22.0 ± 3.0
N4532.....	10B	65	12.14	10.45	4.0	277	−19.19	18.4	−20.82	18.0	26.8	23.0	−20.97	19.2	4	19.6 ± 2.3
N4535.....	5X	42	10.62	8.46	9.9	435	−20.27	15.1	−22.78	17.7	37.0	12.8	−22.06	12.7	4	14.6 ± 2.4
N4569.....	2X	64	9.91	7.45	11.7								−22.76	11.0	1	11.0
N4651.....	5A	59	11.20	8.66	6.1	457	−20.39	20.8	−23.00	21.5	38.4	21.5	−22.94	20.9	4	21.2 ± 0.4
N4654.....	6X	55	10.97	8.80	7.0	377	−19.93	15.1	−22.17	15.6	33.4	16.4	−22.08	15.0	4	15.5 ± 0.6
N4698.....	2A	68	11.24	8.40	6.5	461	−20.41	21.4	−23.03	19.3	38.6	20.3	−23.64	25.6	4	21.7 ± 2.7

B. Cumulative Distance Estimates

Method	No.	μ_V	St. Dev.	Mean Dev.	D (Mpc)
$B-W$	11	31.10	±0.43	±0.13	16.6
$H-W$	13	31.24	±0.53	±0.15	17.7
$A-W$	15	31.18	±0.54	±0.14	17.2
$B-H$	15	30.98	±0.61	±0.16	15.7
All	42[a]	31.12	±0.54	±0.08	16.8

[a] Number of estimates which are independent.

distances of galaxies in and near the Virgo Cluster which matter.

Distances can be estimated for 19 galaxies within the 6° Virgo Cluster, in most cases by more than one method. Not all the methods are independent. If two methods are used, one is semidependent, and we claim $1\frac{1}{2}$ independent measurements. If four methods are used, then two are independent, two are semidependent, and we claim three independent measurements. We have 54 distance measurements of cluster members, 42 of them independent. Our results are summarized in Table 1.

The distance to the Virgo Cluster is determined to be $D_V = 16.8 \pm 0.6$ Mpc ($\mu_V = 31.12 \pm 0.08$), where the error is the standard deviation of the mean of the independent distance estimates and does not account for zero point uncertainty. Coupled with a cluster systemic velocity of $V_V = 1004 \pm 53$ km s^{-1} (see Appendix A), then the local Hubble value is $H_V = 60 \pm 4$ km s^{-1} Mpc^{-1}. This value is consistent with a higher value determined by one of us earlier (Tully and Fisher 1977) because, here, the Hyades are assumed to be 13% farther away and the Virgo systemic velocity is taken to be 10% lower.

c) *Distances to Galaxies in the Virgo II Cloud*

Data are available which provide velocity independent distances for 22 galaxies in the region of the Virgo II Cloud that is being studied. The results are summarized in Table 2. In 14 cases, there was at least one, and frequently several, quality distance estimates. In eight other cases which are identified, the distances are in some doubt because either photometric data are lacking, or the H I profiles are of poor quality, or the galaxies are viewed more face-on than 45° and projection uncertainties are substantial.

The velocity-distance Hubble diagram is plotted for these galaxies and for the Virgo Cluster as an ensemble in Figure 3. The usual strong correlation between redshift and distance is not seen, except relative to the background galaxies around 35 Mpc. In particular, there are numerous galaxies beyond the Virgo Cluster with *lower* velocities than the cluster mean, and, conversely, there are galaxies in front of the cluster with higher velocities. If the relative distances are correct, the line-of-sight deviations from Hubble flow velocities can amount to 700 km s^{-1}. Uncertainties in the observed velocities are negligible in comparison. *The errors that must be ascribed to distances to fit a uniform Hubble flow are much larger than the claimed uncertainties.*

d) *A Point-Mass Infall Model*

We must explain the existence of galaxies with large negative velocities with respect to the Virgo Cluster which are at or beyond the Virgo distance, and of galaxies with large positive velocities which are no farther than the Virgo distance. Infall toward the cluster provides a natural explanation since there is an evident concentration of matter in the vicinity. If there is as much mass in the cluster as the virial theorem would imply (Appendix C), then a region of infall is anticipated. We wish to specify the mass distribution which could account for the amplitude of the observed motions through accumulated gravitational action over the life of the universe. More exotic

TABLE 2

INDIVIDUAL DISTANCE ESTIMATES FOR GALAXIES OUTSIDE THE 6° VIRGO CLUSTER

								$B-W$		$H-W$		$A-W$		$B-H$			
NAME	T	i	V_0	$B_T^{b,i}$	$H_{-0.5}$	a	W_{20}^i	$M_T^{b,i}$	D_{BW}	$H_{-0.5}^{abs}$	D_{HW}	A_{Ho}	D_{AW}	$H_{-0.5}^{abs}$	D_{BH}	METH.	$\bar{D}$
HIGH QUALITY DISTANCE DETERMINATIONS																	
N4116	8B	55	1177	12.25	10.65	5.1	287	−19.27	20.1	−20.98	21.2	27.5	18.5	−20.76	19.2	4	19.7 ± 1.2
U7178	10	48	1205			2.5	128					15.4	21.1			1	21.1
U7332	10	54	805			3.5	124					15.1	14.7			1	14.7
N4273	5B	49	2238	12.20		3.4	400	−20.07	28.5			34.9	35.1			2	31.8 ± 4.7
U7512	10	75	1379			1.9	90					12.0	21.6			1	21.6
U7612	9B	62	1452			3.4	219					22.6	22.8			1	22.8
U7685	8B	48	1405	12.58	11.62	5.4	238	−18.82	19.1	−20.17	22.8	24.1	15.3	−19.28	15.1	4	18.1 ± 3.6
N4517	6A	85	1004	10.10		12.7	318	−19.52	8.4			29.6	8.0			2	8.2 ± 0.3
N4527	4X	70	1618	10.89		7.5	408	−20.12	15.9			35.3	16.1			2	16.0 ± 0.2
N4536	4X	59	1688	10.62	8.30	8.9	394	−20.04	13.5	−22.36	13.5	34.5	13.3	−22.43	14.0	4	13.6 ± 0.3
N4592	8A	77	954		10.55	6.9	213			−19.69	11.2	22.3	11.0			2	11.1 ± 0.1
N4713	7X	52	560	12.02	10.44	4.7	245	−18.89	15.2	−20.29	14.0	24.6	17.9	−20.72	17.0	4	16.0 ± 1.8
U8041	7B	54	1218			5.3	250					24.9	16.1			1	16.1
N4808	6A	67	668		9.96	3.9	292			−21.06	16.0	27.9	24.5			2	20.2 ± 6.0
LOW QUALITY DISTANCE DETERMINATIONS																	
N4123	4B	43	1207	11.77		5.9	309	−19.45	17.6			29.0	16.8			2	17.2 ± 0.5
N4420	5	63	1557			3.4	251					25.0	25.2			1	25.2
N4423	9	90	984			3.4	187					20.2	20.4			1	20.4
U7911	9B	48	1066			4.3	160					18.1	14.4			1	14.4
U7943	5	41	743			3.8	203					21.5	19.3			1	19.3
N4701	6A	38	624	12.69		5.2	300	−19.38	26.0			28.4	18.7			2	22.3 ± 5.1
U8263	5B	90	2949			2.0	195					20.9	35.7			1	35.7
U8285	9	84	825			3.1	143					16.7	18.4			1	18.4

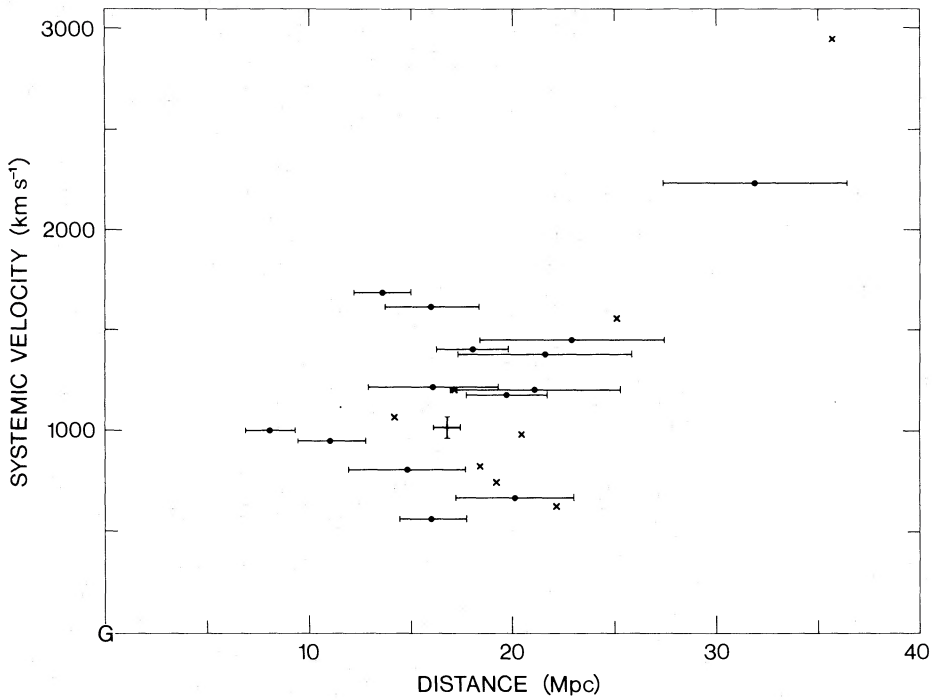

FIG. 3.—A redshift-distance diagram. The point with error bars in both dimensions locates the Virgo Cluster. Positions and velocities associated with individual galaxies projected against the Virgo II Cloud are also plotted. The eight crosses without error bars carry lower weight. The individual error bars are $\pm 20\%/\sqrt{n}$ in distance, where n techniques were used to derive an individual distance.

models may also conform to the observations but are not required.

In a general way, the approach that is followed in our analysis resembles the approach by Hoffman, Olson, and Salpeter (1980) and Hoffman and Salpeter (1982; see also Capelato *et al.* 1982). There are some differences, however. We found it instructive to abandon the convention which involves parameterization in terms of H_0 and Ω and, instead, work in terms of the age of the universe and mass within shells. We assume spherical symmetry for the mass distribution, which permits us to ignore the rest of the universe. Consequently, our models can only indirectly be associated with the large-scale properties of the universe.

When it comes to a comparison with the data, we will look in detail at the circumstances in the specific region close to the cluster that was already discussed, whereas Hoffman *et al.* incorporate data from the central cluster to the edges of the supercluster. We do not consider shell-crossing because in the sample that we are considering *we do not see evidence for a substantial number of galaxies expanding away from the cluster.* Specifically, the vast majority of the galaxies that are close to the cluster in the Virgo II Cloud are tightly clumped and segregated on the sky according to velocity (Fig. 2*b*). We assume that all the galaxies in our Virgo II sample are collapsing for the first time toward the Virgo Cluster. In the model fits, Hoffman *et al.* use a broad brush while we focus on details. It will turn out that our results are consistent and complementary.

Within the precepts of general relativity and assuming spherical symmetry, the detailed structure of the velocity field near the cluster is dependent on four parameters: the duration of time that galaxies have been accelerated by the cluster (the age of the universe, t_0); the total mass of the cluster, M; the mass distribution outside the cluster, dM/dR; and the value of the cosmological constant, Λ. Initially, we will compare the observations with models which utilize only *two* free parameters. For the moment, we take $\Lambda = 0$ and assume that all the mass in the supercluster is within the 6° Virgo Cluster. As the discussion progresses, it will be seen that, although it is not yet possible to define a unique model, there are rather substantial constraints imposed on the four parameters t_0, M, dM/dR, and Λ.

Our point mass model is a special case of distributed mass models which assume spherical symmetry. The standard parameterized equations describing a bound shell are utilized:

$$r = (r_{\max}/2)(1 - \cos \eta) , \tag{5}$$

$$t = (r_{\max}^3/8GM)^{1/2}(\eta - \sin \eta) . \tag{6}$$

The shell reaches maximum expansion at a radius $r = r_{\max}$ when $\eta = \pi$, and reaches full collapse when $\eta = 2\pi$ after a time: $t_c = \pi(r_{\max}^3/2GM)^{1/2}$.

An example is shown in Figure 4 of the velocity perturbations expected according to our model. This case turns out to provide an acceptable fit to the observations. A galaxy located along a specific line of sight with respect to the center of the Virgo Cluster would have a systemic velocity prescribed by its distance as specified in the figure. The turnover in velocity is determined by competition, as one moves toward the cluster, between the monotonically increasing velocity vector directed toward the cluster and the decreasing component that is aligned toward us. For lines of sight sufficiently close to the Virgo Cluster, there may be three separate distances associated with the same observed velocity. This ambiguous situation is referred to as the triple-value problem (Tonry and Davis 1981).

If a galaxy is at a distance which would place it on the heavy portion of a curve in Figure 4, then that galaxy is falling toward the Virgo Cluster and will enter the cluster in less than a Hubble

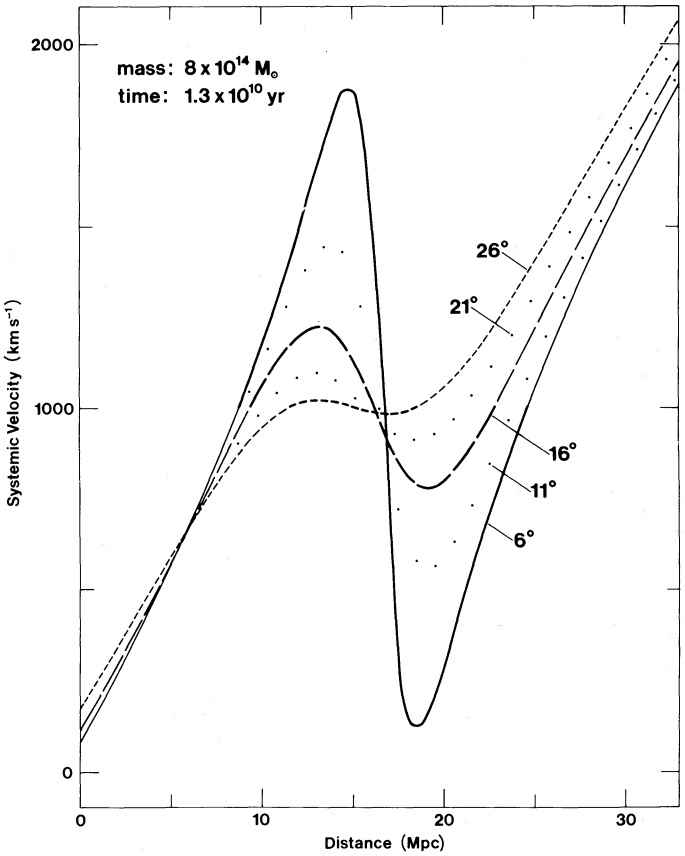

FIG. 4.—The loci of velocities in a redshift-distance diagram predicted by a specific mass-age model. The separate curves indicate the velocities that are anticipated along lines of sight which range from 6° to 26° offset from the center of the Virgo Cluster. If a galaxy lies along the heavy portion of a curve, then it is falling toward the cluster today. There can be three distances along a line-of-sight corresponding to the same systematic velocity: the triple-value ambiguity.

time. With the specific model illustrated, only galaxies within 28° of Virgo could potentially be in the collapse phase today. The turnaround radius, in this case, is at 8 Mpc from the center of Virgo. If a galaxy suffers the triple-value ambiguity, there are always *two* distances it could be at which are associated with infall and *one* distance which corresponds to a location outside the turnaround radius.

We turn our attention now to a comparison between the observations and the models. If only we can distinguish whether a galaxy is at one of the two locations associated with infall rather than at the position associated with continued expansion, then it will prove possible to constrain the models. Galaxies along a given line of sight that lie *within the infall domain* will scatter in observed velocity *below the turnover value. A given mass-age model specifies an envelope to the infall velocities as a function of the line of sight.*

Consider, first, those galaxies in the Virgo II sample with systemic velocities less than 900 km s^{-1}. All such galaxies with distance estimates listed in Table 2 are located near the Virgo Cluster or beyond it. Upon inspection of photographs, we were led to conclude that *all* of the galaxies represented by closed circles in Figure 2*b* (galaxies in Virgo II which are blueshifted with respect to the mean cluster velocity) are at roughly the Virgo distance, rather than a factor of 2 closer. All of these galaxies would be at one of the two infalling locations on the triple-value curves of Figure 4. Foreground contamination among the low-velocity galaxies in the Virgo II sample is negligible.

The situation is not quite so clear on the high-velocity side. In the interval 1000–1700 km s^{-1}, there are galaxies listed in Table 2 with distances both less than the Virgo distance and greater than the Virgo distance. Those that are measured to be closer than, or essentially at, the Virgo distance are presumed to be within the infall regime, but those that are apparently well behind Virgo are taken to be still in the expansion regime.

We do not have good distance estimates for a majority of our sample. Again, it was often necessary to *guess* whether a galaxy was at one of the infall (near) locations or the expansion (far) location from inspection of photographic material. We concluded that 15 high-velocity galaxies were in the infall domain (the open circles in Fig. 2*b*) and 11 were in the expansion domain (identified by letters in Fig. 2*b*). By the happenstance of velocities and positions, our analysis turns out to be *insensitive* to errors in these assignments. With only two exceptions, all galaxies with $V_0 > 1700$ km s^{-1} are taken to be to the background, most associated with Virgo W. Our analysis *would* be affected if any of these galaxies were taken to be near Virgo, but the chances of a factor 2 misassignment of distances in these cases are small. The two exceptional cases of infalling galaxies with redshifts greater than 1700 km s^{-1} are NGC 4532 and UGC 7739, each right on the edge of the 6° Virgo Cluster.

With the identification of a sample of galaxies within the Virgo II Cloud which are falling inward toward the Virgo Cluster, it is possible to specify combinations of the cluster mass and the age of the universe which are compatible with the observed motions. Examples of the model fits are illustrated in Figure 5. Two cases are shown. In Figure 5*a*, the velocities that are plotted are taken with respect to the unweighted mean cluster velocity (Appendix A). It can be seen that there is an offset between the envelope of the open circles (the low-velocity galaxies) and the envelope of the filled circles (the high-velocity galaxies). Fits have been made to these two envelopes separately, and representative cases are illustrated by the solid curves.

The curves map the *extremum* model velocity as a function of the line-of-sight angle from the center of the Virgo Cluster (see Fig. 4) which follows from a specification of the cluster mass and the age of the universe. Since most galaxies along a line of sight would have less than the extremum velocity, points would scatter between the envelope velocity and zero in Figure 5. The two separate envelopes in Figure 5*a* provide what we will call "conservative" upper and lower mass and age limits. As an aside, the small dots in boths versions of Figure 5 represent galaxies which are thought to be beyond the Virgo Cluster, in the expansion region, and consequently should be ignored in this analysis. However, it is seen that these points all fall below the envelope, so if we were in error about their locations, it would be of no concern.

In order to bring both the low-velocity and high-velocity infalling galaxies in line with a single model, we searched for a cluster velocity reference frame which would cause the two envelopes to match up. A shift of 170 km s^{-1} from the observed mean redshift, to 1174 km s^{-1}, was required to give the match shown in Figure 5*b*. If we accept this displacement, it can be rationalized in any of three ways. (*a*) The statistical uncertainty in the mean cluster velocity is 53 km s^{-1}, so a significant

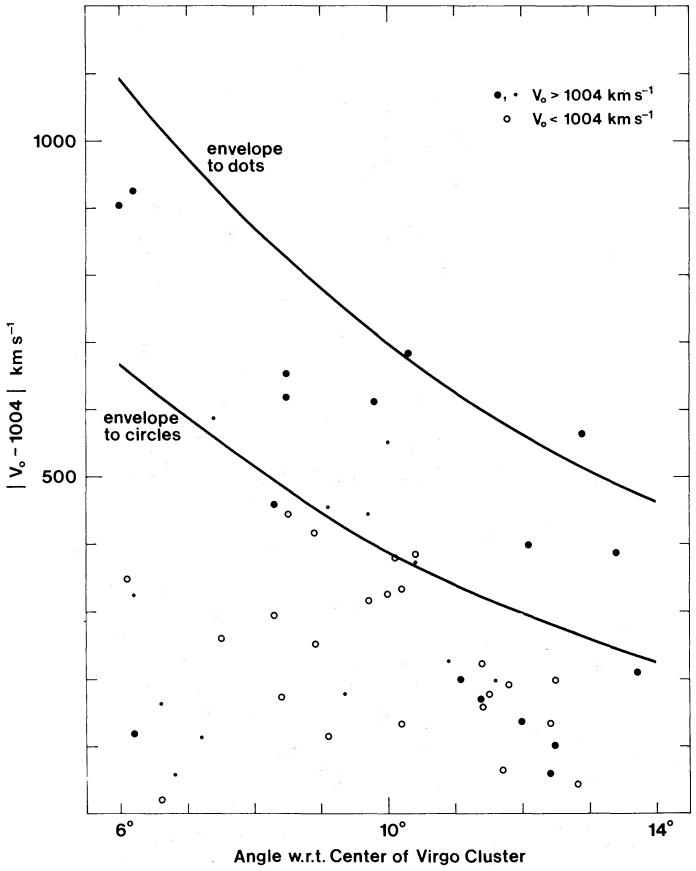

FIG. 5a

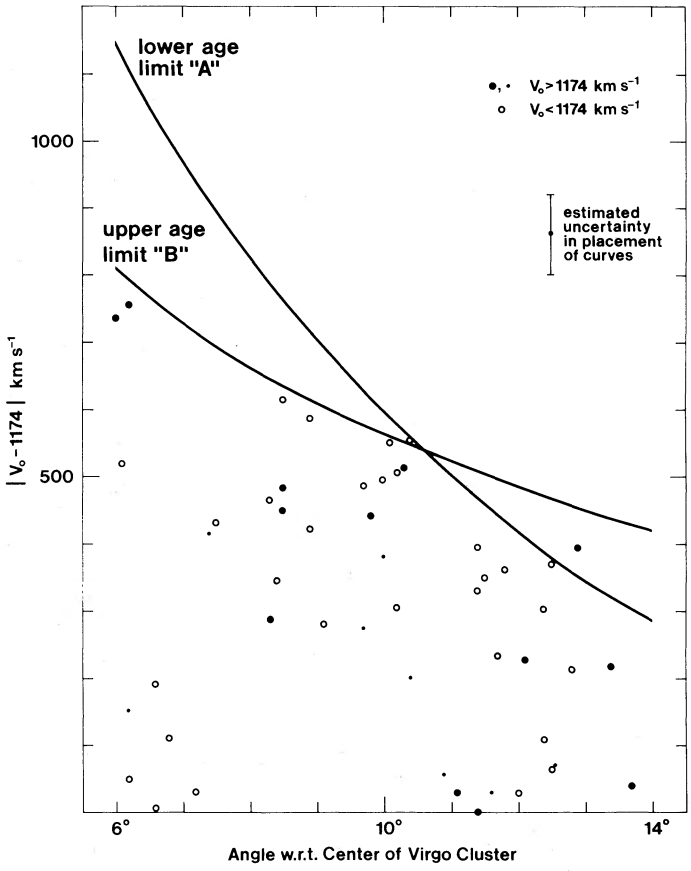

FIG. 5b

FIG. 5.—(*a*) Projected infall velocities, assuming a cluster velocity of 1004 km s^{-1}. *Open circles*, galaxies falling toward the cluster and toward us; *large dots*, galaxies falling toward the cluster but away from us; *small dots*, galaxies expanding away from the cluster and us. Separate models were fitted which provide separate upper envelopes to the distribution of open circles and dots. (*b*) Projected infall velocities, assuming a cluster velocity of 1174 km s^{-1}. The symbols have the same meanings as in Fig. 5*a*. The two solid curves represent fits by two limiting mass-age models. Limit A: $M = 18 \times 10^{14}\ M_\odot$, $t_0 = 6$ Gyr. Limit B: $M = 5 \times 10^{14}\ M_\odot$, $t_0 = 50$ Gyr.

fraction of the 170 km s^{-1} difference could be spurious. (*b*) It is noted that the systemic velocity of M87 is 1181 km s^{-1}, only 7 km s^{-1} different from the shifted cluster velocity. If this dominant galaxy is at rest at the bottom of the potential well of the cluster, then its velocity may have more physical significance and the observed mean velocity may be deviant because of the evolving nature of the cluster. (*c*) The infalling galaxies may have nonzero orbital angular momentum. To explain a 170 km s^{-1} effect, the galaxies in question would have had nonradial velocities of about 130 km s^{-1} when they were at their turnaround radius of 5 Mpc. Perhaps just the single cloud of galaxies that we are studying has net angular momentum, or perhaps these systems are participating in a supercluster-wide rotation. The sense of the purported orbital motion is in agreement with the supercluster rotation claimed to be seen by de Vaucouleurs (1958, 1972) and in sense and amplitude with that claimed by Aaronson *et al.* (1982)—where those analyses were most strongly influenced by the motions of galaxies in Coma–Canes Venatici–Ursa Major. This point is taken up again briefly in Appendix A. If any of the above three explanations is valid, then it is justified that a single envelope be fitted to both the low-velocity and high-velocity galaxies in Figure 5*b*.

Two mass-age cases are illustrated in this figure. Within the restrictions of the point-mass assumption and $\Lambda = 0$, the dependence of infall velocity on distance from the cluster is a strong function of the choice of the mass-age model. The two curves that are plotted demonstrate two extreme circumstances. The steep slope is given by a high mass, low age model, and the shallow slope results from a low mass, large age model. Within the context of the point mass and $\Lambda = 0$ assumptions these models are limiting cases, and are referred to as lower age limit A and upper age limit B, respectively.

The locus of optimum models is demonstrated in Figure 6. The two solid curves represent the limits on the best fits consistent with the error bars shown in Figure 5*b*. The dashed curves illustrate the run of "conservative" fits required by the data in Figure 5*a*. The curves are bounded by the age limits A and B discussed above.

The general trend of the best fit mass-age locus can be understood qualitatively. Peculiar velocities are acquired by an acceleration proportional to mass M, through the age of the universe t_0. Though the relationship between peculiar and infall velocities is complicated, with times around 10 Gyr the locus of our best fit models obeys $M \sim t_0^{-1}$. In the limit of large ages, the galaxies are effectively falling from infinity, and infall velocities are given simply by equating kinetic and potential energy. Hence the models asymptotically approach a constant mass for large ages.

One can comprehend the radial dependence of infall velocities on the choice of mass-age model (i.e., the differing slopes of the envelopes in Fig. 5*b*) if one considers the standard

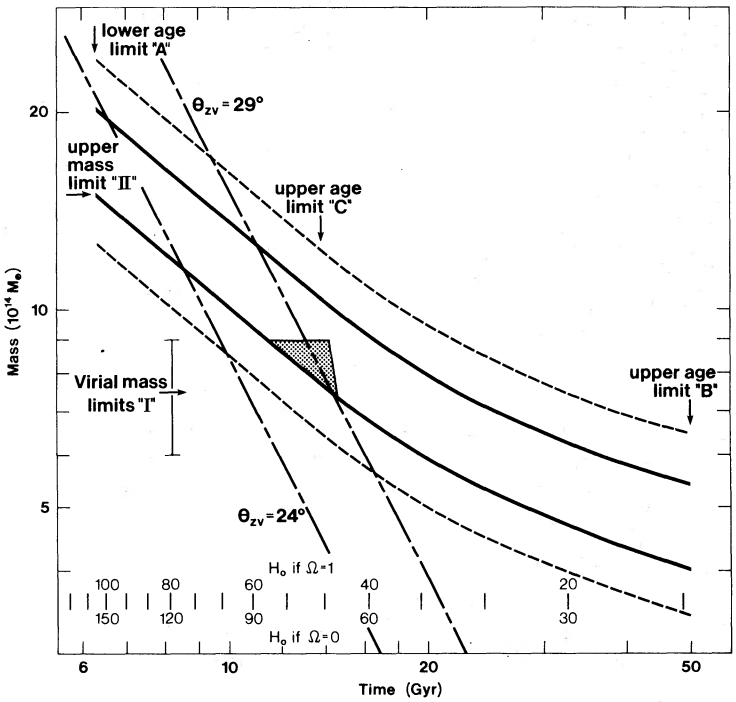

FIG. 6.—The mass-age family of models which satisfies the observed infall motions. The two solid curves correspond to models which give fits to the data displayed in Fig. 5*b* which are offset from the best fit by the amounts shown by the error bars. The dashed curves correspond to models in agreement with the "conservative" fits in Fig. 5*a*. Age limits A and B are set by the acceptable range of the slopes of the curves in Fig. 5*b*. Age limit C is established by the requirement that the model not have too great an influence on motions at the position of the Local Group. Mass limits I are given by the virial analysis of the Virgo Cluster. Mass limit II is a projection of the upper limit given by the virial analysis for the mass within 6° of Virgo to a radius of 10° characteristic of the infalling galaxies, assuming density falls off as $1/R^2$. The two sloping parallel lines correspond to the 24° and 29° limits for today's turnaround radius cited by Hoffman, Olson, and Salpeter.

formula relating collapse time and density for a spherical configuration: $t \sim (R^3/M)^{1/2}$, whence $R \sim t^{2/3}M^{1/3}$. Consider the location of the turnaround radius R_m for different assumed values of the present epoch, t_0. For low age universes, $M \sim t_0^{-1}$ so $R_m \sim t_0^{1/3}$. In the limit of very large age universes, $M \neq M(t_0)$, so $R_m \rightarrow t_0^{2/3}$. In any event, the turnaround radius depends on the choice of the age of the universe: it is greater if the universe is older.

In a young universe, the region we are studying in Virgo II is *relatively near* the turnaround radius, and hence differential infall velocities are substantial. In an old universe, the turnaround radius is farther out, the differential effects across the limited region we are studying are small, and the envelope in Figure 5*b* has a shallow slope.

e) Extended Mass Models

So far, the range of acceptable models is not very restrictive, but we can do better. The fits that have been demonstrated satisfy a sample drawn from a region of limited radial extent from Virgo. Ultimately, motions over the entire supercluster should be considered, but for the moment we introduce only one other observational constraint: the velocity of our Galaxy with respect to the Virgo Cluster.

In Figure 7, we plot the *predicted mean velocity of the Virgo Cluster that we would measure* if the only perturbation to the motion of our Galaxy is due to the point mass in Virgo, for the run of best-fit mass-age models between age limits A and B. Models with the universe 10–15 billion years old predict motions at our position in good agreement with the observed 1000 km s^{-1} motion of the Virgo Cluster *with the point mass*

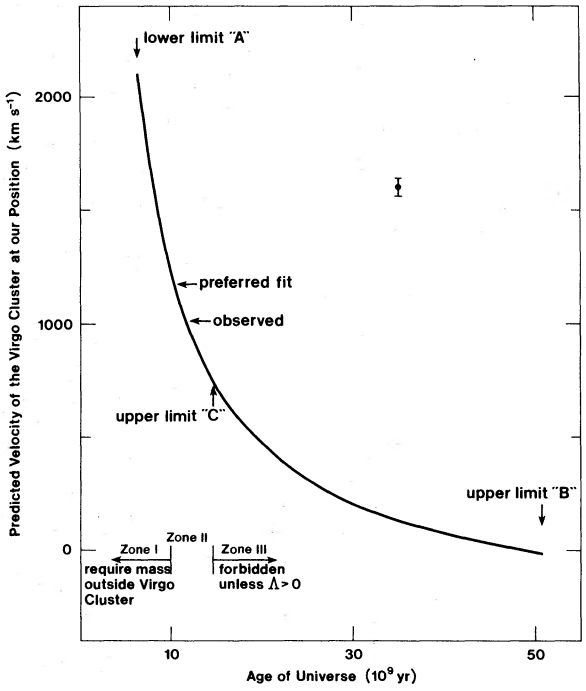

FIG. 7.—The systemic velocity of the Virgo Cluster viewed at the position of the Local Group predicted by the best-fit mass-age models. If $t_0 < 10$ Gyr, then mass is required outside the infalling galaxies which define our models but inside the radius of the Local Group. If $t_0 > 15$ Gyr, then "negative" mass is required in this domain. The error bar indicates the shift associated with the separate models which corresponds to the solid curves in Fig. 6.

approximation. Models with $t_0 < 10^{10}$ years, which satisfactorily describe motions in the Virgo II sample, fail to influence us satisfactorily. A substantial amount of mass is required at radii between Virgo II and our Galaxy. Models with $t_0 > 15 \times 10^9$ years have *too much* influence at our position. Something to counteract the influence of the mass in Virgo would be needed between Virgo II and ourselves: for instance, the cosmological constant could be greater than zero. *If we want to maintain that* $\Lambda = 0$ (or not deny general relativity), *then we are given a very restrictive upper age limit*: $t_0 < 15$ Gyr. This limit is referred to as age limit C.

There are further constraints. It will be argued in Appendix C that the mass within the 6° Virgo Cluster is reasonably well determined by an application of the virial theorem. The limits imposed by that analysis are indicated in Figure 6 as mass limits I. Of course, there could be mass outside the Virgo Cluster but inside a characteristic radius for our infall sample of $\sim 10°$. Upper mass limit II in Figure 6 was calculated on the assumption that density falls off as the distance from Virgo squared (Yahil, Sandage, and Tammann 1980; Tully 1982) and the mass within 6° is given by the upper limit to the virial mass estimate. It will be shown in Appendix A that the galaxy number count falls off *faster* than this rate in the relevant volume about Virgo.

Finally, there are constraints that come out of the complementary analysis by Hoffman, Olson, and Salpeter (1980; also Hoffman and Salpeter 1982). Hoffman *et al.* defined their models by looking at velocity dispersions as a function of Virgo separation, in an analogous fashion to our fitting procedure that was illustrated in Figure 5. However, since they considered galaxies over a much larger range in distances from the central cluster, they were much better situated to isolate the radius of maximum expansion. They concluded that the projected radius of turnaround at the present epoch is in the range 24°–29°. With our distance scale, these limits correspond to 6.8 and 8.1 Mpc.

If these values are substituted into equation (6), which relates the collapse time scale to the local density, then two limiting curves are defined in the mass-time plane. In Figure 6, the two slanting lines with the dependency $M \sim t^{-2}$ correspond to these limits. It is seen that the new upper limit is even more severe than our modeling constraint that the mass within the radius of the Local Group must exceed the mass known to exist in the central cluster.

The limits imposed strictly by our own analysis lead us to favor solutions within the restricted shaded region in Figure 6. A representative case is compared with observations in Figure 8. Predicted velocities are demonstrated for two characteristic lines of sight. The model curves pass very nearly within all of the distance error bars.

It is to be remembered that the models were defined not just by the data illustrated in Figure 8 but by the larger body of data displayed in Figure 5. At this point, a quick review of the steps that led to the definition of our model would probably be helpful, because the observational foundation is stronger than might be apparent. We have good distances to just a small fraction of our sample, but the distance information is used for a limited purpose only: to demonstrate the existence of galaxies at locations incompatible with Hubble flow but compatible with infall models. Once we accepted the hypothesis that an infall model is viable, we could use a much larger data set to define the actual mass-age constraints. Accurate distances were no longer necessary. We only needed the distance discrimination to choose between the infall and expansion regions for each case in the sample: i.e., choose between distances in the range 5–8 Mpc versus 17–23 Mpc for galaxies with $V < 1000$ km s^{-1} or between distances in the range 9–17 Mpc versus 24–30 Mpc for galaxies with $V > 1000$ km s^{-1}. The situation is particularly clean on the low-velocity side because there seems to be no significant foreground contamination. Once the infalling galaxies have been identified, the envelope to the

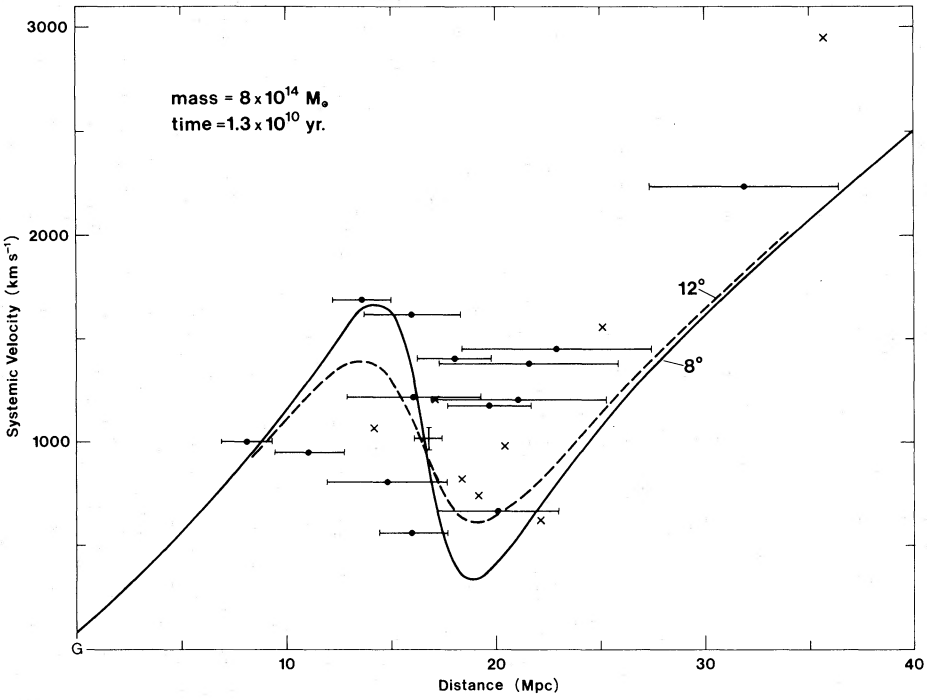

FIG. 8.—The redshift-distance diagram with the predictions of a reasonable mass-age model superposed

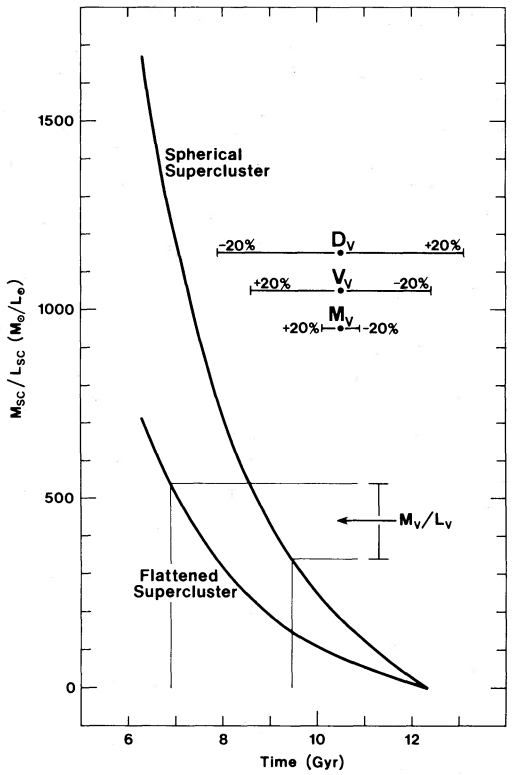

FIG. 9.—The mass-to-light requirement in the supercluster but outside the Virgo Cluster as a function of age for the best fit mass-age models. The mass-to-light ratio found in the Virgo Cluster itself is indicated. Error bars give the age displacement that would occur with 20% variations in the distance scale, the assumed Virgo motion, and the mass of the Virgo Cluster.

streaming motions with respect to the Virgo velocity as a function of the line of sight angle with Virgo restricts the acceptable range of mass-age models. Greater mass or an older universe gives rise to greater excursions.

III. THE COSMOLOGICAL IMPLICATIONS OF THE MASS-AGE MODELS

a) Our Analysis

It was demonstrated in Figure 7 that while only the mass inferred to exist in the 6° Virgo Cluster suffices to explain the observed motion of our Galaxy if the universe is 13 billion years old, in younger universes more mass is required. The situation is illuminated by Figure 9, where the mass-to-light ratio for the supercluster required to explain our ~ 1000 km s^{-1} motion away from Virgo is plotted as a function of the age of the universe. Here, the mass of the supercluster, M_{sc}, is the total mass required *minus* the mass known to exist in the 6° Virgo Cluster ($M_V = 7.5 \times 10^{14}\, M_\odot$; see Appendix C). The luminosity of all galaxies inside our radius in the supercluster, excluding members of Virgo, is $L_{sc} = 7 \times 10^{12}\, L_\odot$. The error bars indicate the horizontal displacement of the curves in Figure 9 that occurs with variations in the assumed parameters: the Virgo Cluster distance, D_V; the Virgo Cluster systemic velocity, V_V; and the Virgo Cluster mass, M_V.

The amount of additional mass required of the supercluster depends on the degree of flattening of the matter,[2] but in any event the increased requirement with decreased age is a very steeply rising function. *No* additional mass is required if $t_0 \sim 13$ Gyr. By comparison, the mass-to-light ratio in the Virgo Cluster determined from a virial analysis (Appendix C) is $M_V/L_V \approx 440$. If one wanted to believe that the mass-to-light ratio is independent of position, then the universe must be only 8 ± 4 Gyr old. The error estimate includes uncertainties associated with the distance scale (± 3 Gyr), a possible peculiar motion of the Local Group (± 2 Gyr), flattening of the supercluster (± 1 Gyr), and the mass of the Virgo Cluster (± 0.4 Gyr).

Going to greater ages, less and less mass is required to explain the motion of the Local Group. At 12.5 ± 4 Gyr, no more mass is required than the cluster virial mass. At greater ages, *less* mass than this amount is required, and models which assume $\Lambda = 0$ do not satisfactorily explain the observations. Taking into account our uncertainties, we would be compelled to conclude that $\Lambda > 0$ if $t_0 > 16.5$ Gyr.

In Figure 10, we demonstrate the values of Λ required to explain our 1000 km s^{-1} motion with respect to the central cluster with a few illustrative assumptions about the mass contained interior to our position in the supercluster. The lowest curve is based on the assumption that the only mass present is the age-dependent "best fit" mass of Figure 6, which is essentially the mass contained in the Virgo Cluster. In another case, the mass is taken to be 5 times greater, since only 20% of the luminosity of the supercluster is contained within the Virgo Cluster (Tully 1982). In a third case, the mass is taken to be 5 times the Virgo Cluster virial mass of 7.5×10^{14} $M_\odot$. Typical values of Λ are $2\text{–}4 \times 10^{-35}$ s^{-2}. All the curves turn over and approach $\Lambda = 3(\dot{a}/a)^2 = 1.1 \times 10^{-35}$ s^{-2} at large times because the density term in the Freidmann equation becomes negligible, but this property is only an academic curiosity since Λ monotonically increases with age in the domain of interest with $t_0 < 20$ Gyr.

The conflict between the Virgo Cluster mass and the mass needed to explain the Local Group motion has been discussed previously. Peebles (1979) assumed a galaxy distribution about the Virgo Cluster similar to the mean distribution around Abell clusters. He then reasoned that the mass-to-light ratio must decrease outside the Virgo Cluster for values of $H_0 < 100$ km s^{-1} Mpc^{-1}. The peculiar velocity of the Local Group would

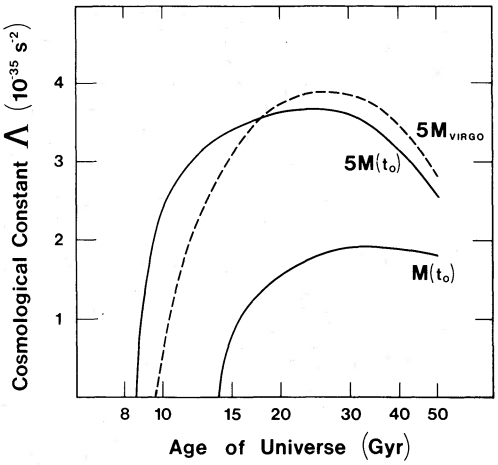

FIG. 10.—The dependence of the requisite value of the cosmological constant Λ with age of the universe given various assumptions about the distribution of mass. The fits assume $V_V = 1004$ km s^{-1} and $D_V = 16.8$ Mpc.

[2] We overestimate the effects of flattening in Fig. 9 because our modeling ignored the background substrate of matter which is important in high-density universes.

otherwise be unacceptably large compared with the reported measured values (Peebles 1976; Aaronson *et al.* 1982).

b) *The Hoffman-Olson-Salpeter Analysis*

Hoffman, Olson, and Salpeter (1980) and Hoffman and Salpeter (1982) demonstrated that the distortion to the Hubble expansion expected at the location of the Local Group, ΔV, is actually expected to be lower in high-density universes, contrary to the intuitive expectation that ΔV would be greater in denser universes (Silk 1974; Peebles 1976). This anomaly arises because there is a rather rigid constraint imposed on the density of the central cluster by the velocity observations, and the *contrast* between this density and the mean density of the background decreases as Ω increases. In other words, the *excess* mass inside the position of the Local Group is lower in a high-density universe.

Of course, the present analysis does not provide us with any information on the parameter ΔV because we ask only how much total mass interior to the position of our Galaxy is needed to explain our observed motion with respect to the Virgo Cluster, V_V. Hoffman *et al.* ask what perturbation is required in a universe of a specified density to explain the observed velocity field and naturally acquire an estimate of ΔV. It is of interest to *couple* the Hoffman *et al.* constraints on ΔV with our constraints on V_V. The standard equation relating the Hubble constant to the age of the universe can be written in the form:

$$t_0 = \frac{f(\Omega) D_V}{V_V + \Delta V - V_p}, \tag{7}$$

where D_V is the distance of the Virgo Cluster, the term V_p allows for our peculiar motion in the line of sight of the cluster, and

$$f(\Omega) = (1-\Omega)^{-1} - \tfrac{1}{2}\Omega(1-\Omega)^{-3/2}\cosh^{-1}(2\Omega^{-1} - 1),$$

so that for $0 \leq \Omega \leq 1$, then $1 \geq f(\Omega) \geq \frac{2}{3}$.

It is possible to solve for the term $f(\Omega)$ by inserting estimates for the other parameters in equation (7). In Appendix A, we determine $V_V = 1004 \pm 53$ km s^{-1}. Aaronson *et al.* (1982) found $(\Delta V - V_p) = 331 \pm 41$ km s^{-1} (the best value for the parameter ΔV alone was 250 ± 64 km s^{-1}). For the age of the universe, we propose $t_0 = 12.5$ Gyr $\pm$ 10%. The upper limit follows from the constraints shown in Figure 6, while for the lower limit we can believe what we are told regarding the ages of star clusters and ages inferred from isotopic abundance ratios ($11 < t_0 < 18$ Gyr: Hainebach and Schramm 1976; Audouze 1980). Let us be optimistic (in the spirit of all these other estimates!) and suppose that the distance scale is sufficiently well established that $D_V = 16.8$ Mpc $\pm$ 10%. Parenthetically, the associated value of the Hubble constant is $H_0 = (V_V + \Delta V - V_p)/D_V = 80 \pm 10$ km s^{-1} Mpc^{-1}. With these values, then:

$$f(\Omega) = 1.02 \pm 0.15 .$$

which requires that $\Omega \lesssim 0.5$.

The uncertainty follows from the face-value acceptance of a number of error estimates in circumstances where substantial systemic effects are possible. Even so, the $\Omega = 1$ case is judged unlikely only at the 2σ level. Consequently, we treat this result as suggestive but hardly compelling evidence for an open universe. The largest uncertainties are in D_V and t_0. Uncertainties in V_V and ΔV would have to be 200 km s^{-1} to be comparable.

A variation of this approach to the definition of Ω is illustrated in Figure 11. Two families of curves are shown, each the result of substitution for $(\Delta V - V_p)$ into equation (7). The standard values $D_V = 16.8$ Mpc and $V_V = 1004$ km s^{-1} are assumed, so we are left with relationships between Ω and t_0. In the case labeled HS, the ΔV values given by the Hoffman and Salpeter (1982) *theoretical* supercluster models (their Fig. 3) are transformed to the (Ω, t_0)-plane, assuming $V_p = 0$. In the case labeled AHMST, the model fits to the *observed* supercluster velocity field by Aaronson *et al.* (1982; their Fig. 5*a*) are reinterpreted in the same manner. In this latter case, the observed parameter is $(\Delta V - V_p)$. This analysis suggests $10.5 < t_0 < 13$ Gyr and $\Omega < 0.4$. The curves would shift on the time scale linearly with modification of the distance scale.

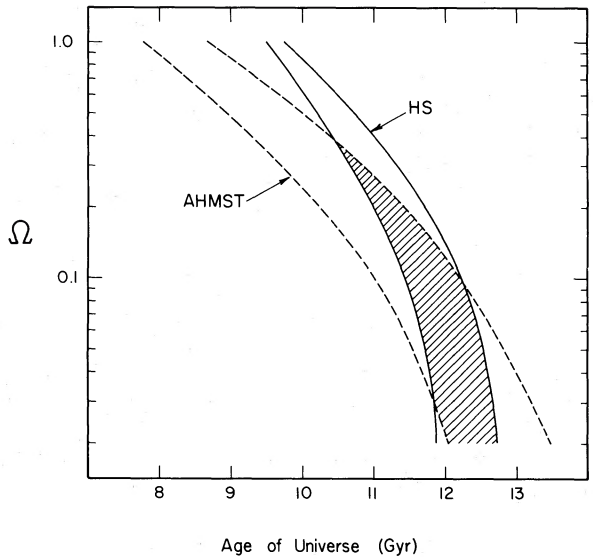

FIG. 11.—Constraints on the density parameter and the age of the universe. The solid curves labeled HS represent transforms of the theoretical $(\Delta V - \Omega)$ relationships determined by Hoffman and Salpeter. The dashed curves labeled AHMST represent transforms of observational limits on $(\Delta V - V_p)$ found by Aaronson *et al.*

Hoffman and Salpeter explored the ramifications of deviations from some of the explicit and implicit assumptions we have made here. They considered departures from spherical symmetry, and models with energy segregation between visible and nonvisible components. In each case, they found only modest (10%–20%) velocity effects. They do warn us that if $\Omega \sim 1$, then ad hoc variations in the distribution of unseen matter can mimic any velocity effect we observe. The amplitudes of these mass variations can be relatively small, so the possibility that they exist cannot be discounted without more knowledge of the details of the local velocity field.

Our two approaches suggest very low values for Ω, somewhat lower values than Davis *et al.* (1980) determined from their modeling of the Local Supercluster (though our results are certainly compatible within the uncertainties). Davis *et al.* utilized the observed local perturbation to the Hubble expansion and the observed overdensity of galaxies in our supercluster to estimate $\Omega \sim 0.4$. Because they were not constrained to a fixed central density, their derived value of Ω was directly dependent on ΔV rather than inversely dependent, and they were forced to assume a direct relationship between the distribution of total mass and the distribution of galaxies.

c) *Summary of Cosmological Constraints*

There are three possible situations. One, but probably only one, of the following statements is likely to be true. (*a*) The universe is less than 10 billion years old (12 Gyr in the limit);

(*b*) the mass-to-light ratio in the supercluster at large is very much lower than it is in the Virgo Cluster core; (*c*) the cosmological constant, Λ, is greater than zero.

Stellar evolutionary models of globular clusters and nucleocosmochronology converge on ages of 11–18 Gyr for the universe (Hainebach and Schramm 1976; Audouze 1980; Janes and Demarque 1983). Within these limits, it is still barely possible to accept models with M/L constant, independent of location in the supercluster. If the universe is closed and M/L increases with distance from the Virgo Cluster, then the local distribution of dark material has perversely conspired to mimic the kinematic effects expected from a low-density universe. Presumably, with more detailed knowledge of the velocity field over a larger volume it will be possible to confirm or discount this possibility. The most probable alternative interpretations of the observations, though, would either require M/L to decrease dramatically with distance from the central cluster or require that the cosmological constant Λ be greater than zero.

IV. THE INFLUENCE OF NEW ARRIVALS ON THE COMPOSITION OF THE VIRGO CLUSTER

a) The Current Infall Rate

Our mass model predicts that galaxies within about 8 Mpc of Virgo have ceased expanding and are falling back toward the Virgo Cluster. Galaxies within this limit must lie in projection within 28° of the center of the Virgo Cluster, in excellent agreement with the conclusions drawn by Hoffman, Olson, and Salpeter (1980). In Figure 4, velocities consistent with our mass model are shown as a function of distance along selected lines of sight.

Galaxies which lie at distances from us corresponding to the heavy parts on the curves in Figure 4 are within the turnaround radius and are now falling toward Virgo. Within the velocity domain of the triple-value problem, there are two distances associated with infall and one distance associated with continued expansion. All galaxies which have stopped expanding will fall into the Virgo Cluster within a Hubble time.

Our goal is to make an inventory of galaxies within the present turnaround point, and to calculate an infall rate. To begin with, we searched the NBG catalog for all galaxies which *might* be falling into Virgo. Candidates had to possess a systemic velocity within the triple-value range consistent with their individual projected separations from Virgo. Only galaxies within 28° of Virgo could qualify, of course, and it is assumed that random motions are small. Some 126 galaxies were identified.

The next step was to try to resolve the triple-value distance ambiguity in each individual case. For 28% of the galaxies, distance estimates were available. For the rest, guesses were made based on morphological considerations and the proximity to objects with more firmly established distances. We accepted 82 galaxies to be within the turnaround radius.

Certainly there will be errors in our distance designations, and individual assignments should not be taken seriously. In particular, there are a substantial number of galaxies near the turnaround radius but taken to be just *outside* it. The Coma I Cluster (de Vaucouleurs' group 13) seems to be just to the foreground in the mean, so we took *everything* in that vicinity to be foreground. Likewise, the group around NGC 5033 and some condensations in the Leo II Cloud (Tully 1982) were taken to be just outside turnaround. There were no substantial entities found just within turnaround as a counterbalance. Although the details regarding individual cases are not to be trusted, the *total number* of galaxies, among those listed in the NBG catalog, that will fall into the Virgo Cluster within the next Hubble time should be defined to within 25%. If anything, our count is likely to be an *under*estimate because of the uncertainties near the turnaround point. It will be argued in § IV*b* that our census is complete to $M_B^{b,i} \approx -19$.

With a resolution of the triple-value ambiguity, our preferred mass model prescribes the correspondence between observed velocity and position. The trajectory of each galaxy can be followed from its present position, and its time of arrival at the boundary of the 6° Virgo Cluster can be estimated. Once inside this boundary, a galaxy can be labeled a member of the cluster. All galaxies which are expected to fall into the Virgo Cluster in the next Hubble time are identified in Table 3. Distances in the table follow from velocities and the mass model.

The histogram shown in Figure 12 summarizes the results on the current rate of influx of galaxies into Virgo. It is seen that the rate will be very substantial over the next 3×10^9 years, but will fall to a low level during the succeeding three-quarters of a doubling of the age of the universe (when $t = 2t_0$). The galaxies which are just now falling into Virgo are, almost all, the members of the Virgo II Cloud discussed earlier. It is seen that this is so in Figure 13. The present location of galaxies due to fall into the Virgo Cluster within the next t_0 years is shown in a view from the pole of the supercluster.

The distribution of galaxies is very clumpy, so the very high rate of infall seen today, or the very low rate expected later, is a happenstance of the details of this distribution. After a little more than a Hubble time in the future, there will again be a considerable infusion of galaxies into Virgo, as regions like Coma I, Leo II, and more of the Virgo II Cloud are pulled in.

b) A Comparison of the Virgo Cluster Population and the Infalling Population

There are 186 galaxies in our velocity sample that are identified with the 6° Virgo Cluster. The distribution in luminosity of the elliptical/lenticular systems and, separately, of the spiral/irregular systems are shown in the open histograms

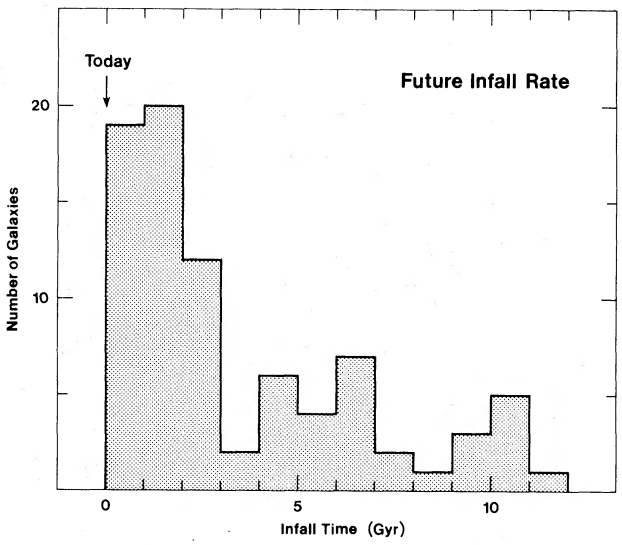

FIG. 12.—Histogram of the rate at which galaxies will be falling into the Virgo Cluster over a doubling of the age of the universe.

TABLE 3

GALAXIES EXPECTED TO FALL INTO VIRGO CLUSTER WITHIN NEXT HUBBLE TIME

NAME	TYPE	$B_T^{b,i}$	$M_B^{b,i}$	DISTANCE (Mpc) to Us	DISTANCE (Mpc) to Virgo	VELOCITY (km s^{-1}) Systemic	VELOCITY (km s^{-1}) Infall	TIME (Gyr) TO ENTER VIRGO
N3455	3	12.53	−18.94	19.7	8.0	987	−32	10.6
N3495	7	11.68	−19.77	19.5	7.9	980	−46	10.2
N3666	5	11.59	−19.50	16.5	4.7	947	−645	2.7
N3705	2	11.11	−20.03	16.9	4.5	891	−708	2.4
N3773	−2	13.01	−18.12	16.8	3.8	904	−905	1.5
N3810	5	11.09	−20.05	16.9	3.6	882	−960	1.4
U6655	13	14.29	−16.92	17.5	3.8	750	−906	1.5
U6670	10	13.10	−18.07	17.1	3.9	838	−873	1.7
U6877	13	13.59	−17.42	15.9	4.4	1050	−720	2.3
N4037	5	12.46	−18.68	16.9	2.1	844	−1584	0.2
N4061	−5	14.21	−16.61	14.6	3.6	1545	−975	1.3
N4065	−5	13.55	−17.50	16.2	3.0	1122	−1186	0.8
N4064	1	11.85	−19.26	16.7	2.6	959	−1353	0.5
N4116	8	12.25	−18.76	15.9	3.3	1177	−1045	1.1
N4123	4	11.77	−19.23	15.9	3.3	1207	−1064	1.1
N4129	5	12.34	−18.53	14.9	6.4	1034	−309	5.5
N4179	−2	11.76	−19.25	15.9	3.5	1144	−984	1.3
U7239	10	13.82	−17.28	16.6	1.8	1126	−1791	0.1
1213−11	10	...	...	16.0	6.9	985	−210	6.9
U7332	10	13.91	−17.27	17.2	3.7	805	−929	1.5
N4293	0	11.19	−19.95	16.9	1.9	824	−1749	0.1
N4303	4	10.05	−20.94	15.8	2.6	1464	−1361	0.5
U7477	13	14.03	−17.73	22.5	6.1	657	−363	4.9
1221+04	−2	14.83	−17.00	23.3	7.1	829	−187	7.3
N4423	9	13.12	−18.00	16.8	1.9	984	−1715	0.1
N4457	0	11.62	−19.55	17.1	2.6	752	−1327	0.6
N4494	−5	10.75	−19.60	11.7	6.0	1289	−373	4.8
N4496	9	11.62	−18.97	13.1	4.3	1625	−763	2.1
1229+04	10	...	...	13.4	4.0	1659	−832	1.8
U7685	8	12.58	−18.23	14.5	4.0	1405	−839	1.8
1230−04	8	...	...	11.3	6.9	1151	−213	6.8
N4527	4	10.89	−19.92	14.5	3.5	1618	−986	1.3
N4532	10	12.14	−18.81	15.5	2.1	1909	−1588	0.2
N4536	4	10.62	−20.00	13.3	4.4	1688	−734	2.2
U7739	10	14.71	−16.21	15.2	2.3	1931	−1480	0.4
N4546	−2	11.23	−19.93	17.1	4.8	882	−633	2.7
N4561	8	12.77	−17.53	11.5	5.6	1430	−458	4.0
N4565	3	9.22	−20.99	11.0	6.6	1213	−260	6.1
N4586	1	12.25	−18.92	17.1	2.5	722	−1401	0.5
N4597	9	11.99	−19.17	17.0	5.4	904	−496	3.7
N4630	9	13.06	−18.16	17.5	2.8	587	−1271	0.7
N4632	5	11.88	−18.89	14.2	4.3	1572	−756	2.1
N4635	7	13.30	−18.61	24.1	7.8	944	−63	9.8
N4636	−5	10.46	−20.68	16.9	3.0	869	−1179	0.8
U7911	9	13.64	−17.40	16.2	3.6	1066	−955	1.4
N4665	0	11.84	−19.36	17.4	3.0	678	−1157	0.9
N4666	5	11.12	−19.62	14.1	4.5	1395	−708	2.4
N4670	0	13.05	−16.91	9.8	7.7	1068	−78	9.4
U7943	5	13.58	−17.58	17.0	2.2	743	−1530	0.3
N4688	6	12.84	−18.29	16.8	2.7	891	−1313	0.6
N4691	3	11.60	−20.18	22.7	8.1	989	−18	10.9
N4697	−5	10.12	−20.39	12.6	6.3	1169	−318	5.4
N4701	6	12.69	−18.96	21.4	5.7	624	−445	4.1
N4713	7	12.02	−19.20	17.5	2.6	560	−1325	0.6
N4725	2	9.89	−20.30	10.9	6.7	1199	−243	6.4
N4747	5	12.79	−17.38	10.8	6.8	1183	−224	6.7
N4753	13	10.79	−20.19	15.7	4.3	1102	−763	2.1
U8011	10	...	...	22.2	6.5	747	−292	5.7
N4758	3	12.90	−18.19	16.5	1.9	1196	−1774	0.1
N4765	1	12.82	−18.89	22.0	6.1	687	−358	5.0
N4771	7	11.89	−19.13	16.0	3.6	1110	−944	1.4
N4772	1	12.23	−18.86	16.5	3.4	982	−1026	1.2
N4810	10	14.35	−17.38	22.2	6.6	779	−260	6.1
N4809	10	14.06	−17.72	22.7	7.1	843	−182	7.3
U8036	5	12.43	−19.44	23.6	7.5	893	−118	8.5
U8041	7	12.21	−18.70	15.2	4.1	1218	−804	1.9
U8053	8	14.04	−17.60	21.2	5.6	621	−456	4.0
N4808	6	12.20	−19.48	21.7	5.9	668	−388	4.6
N4818	2	11.12	−18.95	10.3	8.2	1012	−13	11.1

TABLE 3—*continued*

NAME	TYPE	$B_T^{b,i}$	$M_T^{b,i}$	DISTANCE (Mpc) to Us	DISTANCE (Mpc) to Virgo	VELOCITY (km s^{-1}) Systemic	VELOCITY (km s^{-1}) Infall	TIME (Gyr) TO ENTER VIRGO
U8074	9	14.34	−17.41	22.4	6.9	811	−223	6.7
N4845	1	11.30	−19.80	16.6	3.7	960	−924	1.5
N4880	−2	12.29	−18.73	16.0	2.2	1499	−1552	0.3
N4900	5	12.06	−19.08	16.9	3.6	870	−950	1.4
1302−07	9	...	...	20.7	8.1	988	−26	10.7
N4951	6	11.87	−18.27	10.7	7.8	1048	−68	9.6
N4958	−2	11.30	−20.26	20.5	8.0	984	−33	10.5
U8285	9	14.07	−17.09	17.1	3.4	825	−1026	1.2
U8385	9	13.54	−17.50	16.1	3.6	1079	−947	1.4
N5147	8	12.21	−18.80	15.9	5.0	1020	−596	3.0
U8575	10	14.09	−16.82	15.2	4.8	1122	−634	2.7
U8614	10	13.00	−18.02	16.0	4.9	1004	−604	2.9
N5248	4	10.69	−20.22	15.2	4.9	1112	−604	2.9

in Figure 14. The Virgo Cluster distance modulus was assumed to be 31.12 mag. The sample is complete at least to the level of the Shapley-Ames limit of $B_T = 12.7$ (Sandage and Tammann 1981), so with corrections it should be essentially complete to $B_T^{b,i} = 12.0$, or $M_B^{b,i} = -19.1$. The distribution of galaxies shown in the histograms bolsters our confidence that the sample is complete to at least this limit, and perhaps to 0.5 mag fainter (see also Appendix A).

By comparison, the filled histograms in Figure 14 are the equivalent information on the 72 galaxies that are due to fall into the Virgo Cluster during the next $\frac{2}{3}t_0$ years. It is to be recalled that the distances to these galaxies (and hence the intrinsic luminosities) follow from the resolution of the triple-value problem. Once more, the details may be questioned but the general picture should be correct. As with the cluster sample, the infall sample seems to be complete to about $M_B^{b,i} = -18.5$, corresponding in the mean to about $B_T^{b,i} = 12.5$.

We have integrated from today up to only two-thirds of a doubling of the age of the universe, because there is a large uncertainty in the number of galaxies with infall times near $2t_0$ due to the proximity of several substantial groups to the turnaround radius.

The two samples may be compared at levels above the completion limits (conservatively taken to be $M_B^{b,i} = -19.1$). The infall sample contains 70% as many spirals/irregulars as the Virgo sample, and these galaxies possess 55% of the integrated light of the Virgo spirals/irregulars. By contrast, the infall sample contains ellipticals/lenticulars which number only 14% of the equivalent population in Virgo, and contain

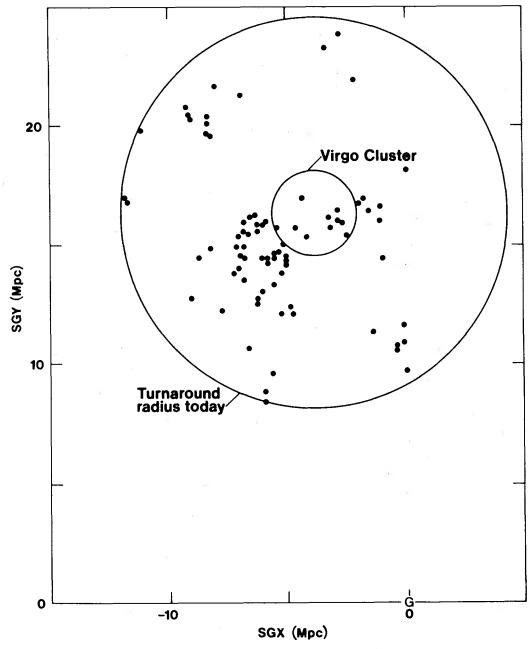

FIG. 13.—A view from the pole of the supercluster of all cataloged galaxies within the turnaround radius today. Galaxies are positioned in conformity with a specific mass-age model. These are the galaxies which will fall into the cluster within the next Hubble time.

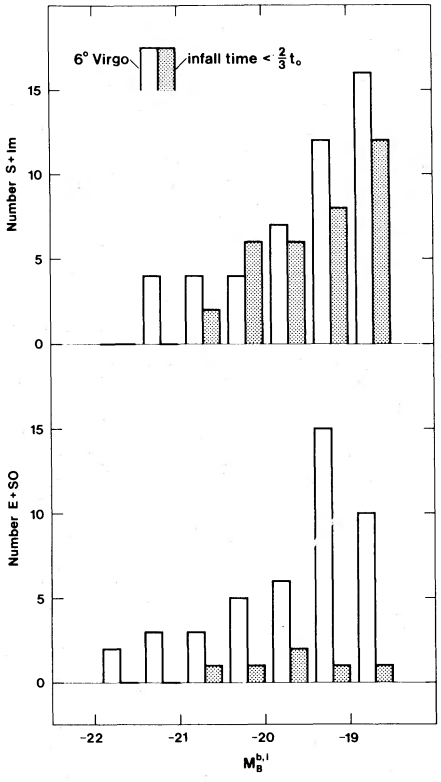

FIG. 14.—Luminosity histograms. *Top*, spirals and irregulars. *Bottom*, ellipticals and lenticulars. *Open histograms*, members of the Virgo Cluster. *Shaded histograms*, galaxies which will fall into the cluster within the next $\frac{2}{3}$ of a Hubble time.

between them only 15% as much integrated light. This infall sample will be integrated into the Virgo Cluster over the next two-thirds of a Hubble time.

The conclusions to be drawn are clear. It is entirely plausible that *all* of the spiral/irregular systems observed in the Virgo Cluster today have been there for significantly less than 10^{10} years. In this case, none of the presently observed gas-rich systems in Virgo would have been first-generation members. On the contrary, the influx of ellipticals and lenticulars has not been too important. These systems are either being created out of spirals and irregulars or they have always been there since the cluster was born.

c) *Summary of Appendix A*

In Appendix A, there is a status report on the state of our knowledge concerning characteristics of the 6° Virgo Cluster. There are discussions concerning (i) mean velocities and dispersions, (ii) radial distributions, (iii) luminosity functions, and (iv) gas deficiencies both for the cluster viewed as an ensemble and for morphological subgroupings. We view all the fine points discussed in that appendix to be compatible with the thesis that the spirals in Virgo are relative newcomers. In particular, given the very clumpy nature of the supercluster medium, it is easy to understand why there could be clumping in the spiral galaxy velocity histogram. Groups of galaxies which arrived in the cluster recently would still collectively retain a memory of a common history. The details could not have been anticipated; only that there would be a lot of kinematic and distributional structure.

The fact that the lenticulars appear not to be confined to the center of the cluster so closely as the ellipticals suggests that their origins might be more closely associated with the spirals. Virgo lenticulars have lower random motions than the gas-rich disk systems which would result if they joined the cluster earlier, with lower infall velocities. They have had more time in the cluster to lose or expend their gas. The mechanisms might have been tidal stripping, direct galaxy collisions, ram pressure stripping by an intracluster medium near the cluster core, thermal ablation by the hot intracluster core, or simply exhaustion via star formation as we will champion in the accompanying paper (Shaya and Tully 1984). The gamut of such properties as H I content and anemic tendencies would be correlated with the length of time a galaxy has been in the cluster.

d) *Remarks*

Tully, Mould, and Aaronson (1982) showed that the colors of lenticulars could be understood as an evolutionary effect if star formation is arrested in a spiral galaxy, say, because all the gas is spent. In a quarter of a Hubble time, the system would evolve in color and luminosity from a "gas-rich" branch where star formation had been occurring to a lenticular branch. The most massive systems would dim about 1 mag in the blue with this transition. If one considers the luminosity histograms in Figure 17, it is plausible, although not compelling, to view the lenticular distribution as a replica of the spiral distribution but dimmed by about a magnitude.

There is one other indirect piece of evidence regarding the past history of accretion into the Virgo Cluster. Hoffman, Olson, and Salpeter (1980) considered collapsing shell models with smoothly varying density distributions and allowed for shell rebounds. They described a characteristic radius of rebound in terms of the turnaround radius at the present epoch, and found that this parameter is sensitively dependent on the ratio of the present age of the universe to the initial collapse time scale of the cluster. In our terminology, this ratio is t_0/t_c. In Appendix C, it is found that the collapse time scale for the *elliptical* galaxies in Virgo is $t_c \sim 2$ Gyr, so $t_0/t_c \sim 6$ (whence the Hoffman *et al.* parameter would be $t/t_1 \sim 12$). With such a large value of this ratio, Hoffman *et al.* would predict expanding shells to reach one-half to three-fourths of the current turnaround radius.

Now, there may well be some galaxies in our sample that have passed through the cluster and are moving outward. However, as argued in § II*d*, we do not feel that there are substantial numbers of such galaxies. From the apparent paucity of outwardly moving galaxies beyond the 6° cluster radius, the Hoffman *et al.* modeling would seem to require a characteristic ratio $t_0/t_c < 1.5$.

The contradiction in these two values of t_0/t_c can most easily be reconciled by supposing that there is nothing like uniform (luminous) density in the collapsing shells. The clumped nature of the galaxy distribution in the supercluster (Tully 1982) encourages that view. A reasonable supposition in the context of these observations would be that the elliptical galaxies and, probably, the lenticular galaxies fell into the cluster on a time scale compatible with the $t_0/t_c \sim 6$ value, while the bulk of the spirals have fallen in on a time scale compatible with $t_0/t_c < 1.5$. In other words, most of the spiral galaxies in the Virgo Cluster have been there for less than 4 Gyr. If so many galaxies fell in so recently, then one could infer from Figure 12 that those galaxies were only the advance part of the same cloud continuing to fall into the cluster today.

This 4 Gyr estimate is consistent with the time scale of ejection of NGC 4569, discussed in Appendix B. If the cluster spirals have arrived relatively recently, this fact would explain a number of the kinematic and distributional characteristics of the cluster discussed in Appendix A. If most lenticulars arrived in the cluster at a distinctly earlier epoch, it might be understood why there is such a discrete separation between spirals and S0 systems in the color-magnitude diagram discussed by Tully, Mould, and Aaronson (1982).

V. RECAPITULATION

A substantial group of galaxies is observed to be falling toward the Virgo Cluster. That fact has lead us to pursue three avenues of research. (*a*) Mass-age models were constructed to describe the observations, and these mass-age models turned out to have interesting ramifications for various cosmological parameters. (*b*) The models were used to predict the near-future rate of galaxy accretion by the Virgo Cluster, and this investigation lead to speculation concerning the evolution of the mix of morphological types in the cluster with time. (*c*) A model will be offered (Shaya and Tully 1984) which explains the segregation of galaxy types in terms of an environmental dependence on the availability of high angular momentum material at the times of galaxy formation.

a) *Mass-Age Models and Constraints on Cosmological Parameters*

1. A family of mass-age models can be defined which satisfactorily explains the infall pattern of radial velocities observed among galaxies in the Virgo II Cloud near the Virgo Cluster. The turnaround radius about Virgo today is at 8 Mpc (28° projected) if the Virgo distance is 16.8 Mpc and the

universe is 13 Gyr old. Galaxies are entering the cluster today with velocities of 1800 km s^{-1}.

2. The constraint provided by the observed motion of the Galaxy with respect to the Virgo Cluster places a requirement on the mass in the supercluster at radii beyond the infalling group. That constraint generates three interesting domains, depending on the age of the universe.

2*a*. If $t_0 < 10$ Gyr (in the limit: 12 Gyr), then it is possible to construct satisfactory models with $M/L \sim$ constant across the supercluster, where the constant is roughly the M/L value found from a virial analysis of the Virgo Cluster. However, the ages of globular clusters and ages implied by the abundance of nuclear decay products appear to conflict with the hypothesis of such a young universe.

2*b*. If $10 < t_0 < 15$ Gyr, then satisfactory infall models can be found that require essentially no more mass than is known to exist in the central cluster from an application of the virial theorem: $M_{vir} = 7.5 \pm 1.5 \times 10^{14}\ M_\odot$. Because 80% of the light in the supercluster lies outside the Virgo Cluster, M/L must drop from $440 \pm 100\ M_\odot/L_\odot$ inside the cluster to perhaps an order of magnitude lower at large in the supercluster.

2*c*. If $t_0 > 15$ Gyr (in the limit: 16.5 Gyr), then *less* than the cluster virial mass is required to consistently explain motions in the infalling cloud and the motion of our Galaxy. If forced to conclude that the universe is older than this limit, then one can resort to models with $\Lambda > 0$ (reasonable value for Λ are $2\text{–}4 \times 10^{-35}\ s^{-2}$).

b) The Virgo Cluster Accretion Rate

1. There will be a 50% augmentation in the number of spirals and irregulars in the Virgo Cluster over the next $\frac{1}{4}t_0$ and a 70% augmentation over the next $\frac{2}{3}t_0$. The infall rate is very irregular because of the clumpy distribution of galaxies in space. A large group is falling into the cluster right now.

2. It is plausible that essentially all of the spirals and irregulars in the Virgo Cluster have arrived significantly more recently than a Hubble time. The spatial and kinematic structure in the cluster, such as the higher velocity dispersion and larger mean radius for spirals (Appendix A), supports that contention. The apparent escape of NGC 4569 from the cluster (Appendix B) suggests that a major coalescence occurred at roughly $\frac{2}{3}t_0$. The fact that there are very few galaxies just outside the 6° cluster that are *not* part of the infalling group further argues that the spiral galaxies in the cluster arrived recently (since there is not a significant number of galaxies which have had time to reemerge).

3. The present influx of ellipticals and lenticulars into the Virgo Cluster is insignificant compared with the number already there. Either the number of these gas-deficient galaxies is growing with time through the conversion of spirals and irregulars into ellipticals and lenticulars, or the present accretion of late-type systems is diluting an environment which was once even more extremely segregated in favor of early morphological types than the present one.

4. The Virgo Cluster might represent the case of an ongoing merger between a cluster composed principally of elliptical and lenticular galaxies and a cloud of spiral galaxies. There is evidence that the merger began about 4 Gyr ago and will continue for the next 3 Gyr.

We thank Bill Saslaw for his ideas concerning the peculiar case of NGC 4569. Financial support was provided by NSF grants AST 79-26046 and AST 82-03971 and by an award to E. S. from the Honolulu Chapter of the Achievement Rewards for College Scientists Foundation.

APPENDIX A

MISCELLANEOUS CHARACTERISTICS OF THE VIRGO CLUSTER

The literature is filled with curiosities regarding the Virgo Cluster environment. It had been suspected once that the mean redshifts of the ellipticals and spirals were different (de Vaucouleurs 1961; de Vaucouleurs and de Vaucouleurs 1973), although, as the samples grew, this difference has ceased to look significant (Sandage and Tammann 1976; Sulentic 1980). De Vaucouleurs and de Vaucouleurs (1973) claimed that Sd-Im galaxies are *blueshifted* with respect to Sa-Sb galaxies in Virgo, while Sulentic (1980) proposed that Sbc-Scd spirals are *redshifted* with respect to Sa-Sb spirals! At least there is agreement that the velocity dispersions of gas-rich systems are greater than those for poor-gas systems (de Vaucouleurs 1961; Tammann 1972); and, in fact, there may be a significant difference in this regard between ellipticals and lenticulars, with the velocity dispersion smallest for lenticulars (Sulentic 1980). Both Helou, Salpeter, and Krumm (1979) and Sulentic (1980) have noted that the differences in velocity dispersions between lenticulars and spirals are most striking in the 3° radius core of the cluster and proposed that this observation is evidence for gas stripping from low velocity spirals. The velocity histogram for the ellipticals plus lenticulars is peaked near the cluster velocity, but for the spirals plus irregulars it is clumpy and broader (see Sulentic 1980), and de Vaucouleurs (1982) has called the spiral distribution bimodal. The elliptical galaxies in Virgo are more concentrated toward the center of the cluster than are the spirals (cf. de Vaucouleurs 1961). Also, there are persuasive claims that the disk systems in Virgo are deficient in neutral gas compared with "field" galaxies of similar types (Davies and Lewis 1973; Krumm and Salpeter 1979; Chamaraux, Balkowski and Gérard 1980; Giovanardi *et al.* 1983). Several of van den Bergh's (1976) anemic galaxies are in the Virgo Cluster.

All of these qualities can be accommodated by the picture of the infall of supercluster galaxies into the Virgo Cluster. In this appendix, we will review these matters in the light of our larger sample, taking care to distinguish between the 6° cluster and the Virgo II Cloud. There remains one perverse set of observations which cannot be reconciled so easily. It has been claimed that at least a few of the low-velocity objects in the line of sight of the cluster are actually in the foreground (Holmberg 1961; Sulentic 1977; McClure, Cowley, and Crampton 1980; de Vaucouleurs 1982). This perplexing possibility will be discussed in Appendix B.

a) Systemic Velocity and Dispersions

Let us return to the sample of 186 galaxies in the Virgo Cluster with published velocities. *All* galaxies with $V_0 < 3000$ km s^{-1} and within 6° of the center of the cluster (taken to be

TABLE 4

MEAN VELOCITIES AND DISPERSIONS OF CLASSES OF GALAXIES IN THE VIRGO CLUSTER

Type (1)	No. (2)	R_Ω (Mpc) (3)	σ_V^* (km s^{-1}) (4)	$V_{V,T}$ (km s^{-1}) (5)	$\lvert V_{V,T} - 1004\rvert$/err (6)
E	30	0.42	678	946 ± 125	0.4
S0	45	0.78	515	1185 ± 78	1.9
S0/a–Sb	43	0.78	793	862 ± 122	1.1
Sbc–Scd	27	0.53	687	1290 ± 133	2.0
Sd–Im	29	0.80	783	935 ± 146	0.4
E + S0	75	0.63	597	1089 ± 70	1.0
S + Im	111	0.79	782	947 ± 75	0.6
All types	186	0.76	716	1004 ± 53	...
−lum. wt	18	0.77	750	958 ± 100	...

Col. (1), subsample. Col. (2), Number of galaxies in the subsample. In the luminosity-weighted case (last line), the "characteristic number" is given: $N_{\rm char}$ = (total luminosity)/(luminosity of brightest member). Col. (3), virial radius: $R_\Omega = \sum_{\rm pairs} m_i m_j / \sum_{\rm pairs} m_i m_j / R_{ij}$. Col. (4), dispersion with respect to the mean velocity of the subsample. Col. (5), mean velocity of the subsample. Col. (6), significance of the deviation of the subsample mean velocity from the ensemble mean velocity. The standard deviation error in the divisor includes the uncertainty in the ensemble mean velocity as well as the uncertainties in the subsample means.

coincident with M87) are accepted in this discussion. Our results concerning the kinematic properties of the cluster are summarized in Tables 4 and 5 and Figure 15.

In Table 4, there is information on mean velocities, velocity dispersions, and radii associated with various subsets of the sample. In all but the last case in this table, galaxies are given equal weight in the solutions. The last case involves luminosity weighting. The *disadvantage* of luminosity weighting is that relatively few galaxies in the sample contribute to the results (Bahcall and Tremaine 1981). A measure of the number of galaxies influencing a solution is given by the characteristic number, $N_{\rm char}$ (defined in notes to Table 4). Whenever we attempted luminosity weighted solutions, $N_{\rm char}$ would be around 10% of our sample size. If energy equipartition is unimportant, the velocities of large and small galaxies will be similar, and an unweighted solution is to be preferred because the sample will be largest. Equipartition of energy would lead to lower velocity dispersions for more massive galaxies; but since the luminosity weighted sample (dominated by the biggest systems) has a *higher* velocity dispersion than the unweighted sample, there is no evidence of significant equipartition.

Our best estimate of the systemic velocity is given by the

TABLE 5

VELOCITY DISPERSIONS OF CLASSES OF GALAXIES IN THE VIRGO CLUSTER

A1. EVIDENCE THAT $\sigma_V^{S,I} > \sigma_V^{E,L}$

	$E+L$		$S+I$		
RANGE	No.	σ_V	No.	σ_V	SIGNIFICANCE
Entire cluster	75	614 ± 48	111	792 ± 44	2.7 σ
0°–3°	37	686 ± 66	44	920 ± 69	2.5 σ
3°–6°	38	544 ± 68	67	703 ± 55	1.8 σ

A2. EVIDENCE THAT $\sigma_V^{S,I} > \sigma_V^{L}$

	L		$S+I$		
RANGE	No.	σ_V	No.	σ_V	SIGNIFICANCE
Entire cluster	45	557 ± 56	111	792 ± 44	3.3 σ

B. EVIDENCE THAT LINE-OF-SIGHT VELOCITY DISPERSION FALLS WITH RADIUS

	ALL GALAXIES		
RANGE	No.	σ_V	SIGNIFICANCE
0°–3°	81	816 ± 50	...
3°–6°	105	636 ± 43	2.7 σ

NOTE.—(*a*) Velocity dispersions are with regard to ensemble mean velocity of 1004 km s^{-1}. (*b*) Significance = difference/$(\sigma_1^2 + \sigma_2^2)^{1/2}$.

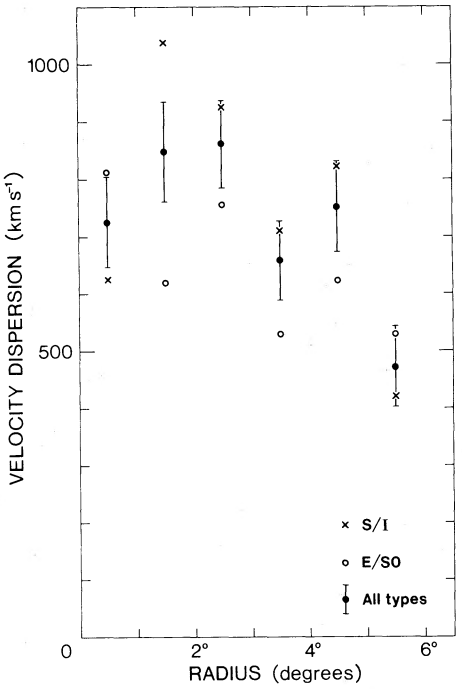

FIG. 15.—Velocity dispersion as a function of radius in the Virgo Cluster

unweighted average of all 186 galaxies: $V_V = 1004 \pm 53$ km s^{-1}.[3] This result is in close agreement with the luminosity weighted value of 1019 km s^{-1} given by Mould, Aaronson, and Huchra (1980). The mean velocities of various subsamples are shown in Table 4. We do not find significance in any of the departures from the favored cluster velocity of 1004 km s^{-1}.

The velocity dispersions recorded in Table 4 are measured with respect to the mean velocities of the respective samples, $V_{V,T}$ (subscript T stands for type). By contrast, the velocity dispersions in Table 5 are measured with respect to $V_V = 1004$ km s^{-1}. These latter dispersions are more meaningful if it is correct that the fluctuations in $V_{V,T}$ about V_V are merely statistical. Two conclusions can be drawn: (*a*) The dispersion of the lenticulars seems to be significantly less than the dispersion of later-type disk systems, and (*b*) there is some evidence that velocity dispersions fall with distance from the center of the cluster. Figure 15 illustrates the weak dependence of dispersion on radius.

The suggestion was raised during the discussion of Figure 5*b* that there may be significant orbital angular momentum associated with the infalling galaxies. The sense of that purported orbital motion is in agreement with earlier assertions that the supercluster is undergoing rotation (de Vaucouleurs 1958, 1972; Aaronson *et al.* 1982). Recent arrivals in the Virgo Cluster might have contributed a detectable amount of net angular momentum. To test this hypothesis, the cluster was divided at the supergalactic longitude of M87 and the mean velocities of the galaxies of the two halves were compared (ellipticals were excluded). The 81 disk galaxies with SGL > 102.9 had a mean velocity of 1129 ± 70 km s^{-1} while 75 disk galaxies with SGL < 102.9 had a mean velocity of 892 ± 93 km s^{-1}. The difference of 237 ± 116 km s^{-1} is only a 2 σ result, but the sense of the difference is in agreement with the observations of rotation. Since galaxies in the cluster have fallen in from just a few megaparsecs, tangential velocities would be only a factor of about 2 greater than they were at turnaround, and it is understandable that the effect would be difficult to see in the noise of the large random motions of the cluster. Helou and Salpeter (1982) report that the spin axes of individual galaxies in the cluster may have a preferential orientation. Their result has only a 1 σ significance, but the alignments of the proposed spin and orbital angular momentum vectors are the same.

[3] Corrected for solar motion of 300 km s^{-1} toward $l = 90°$, $b = 0$.

TABLE 6

RADIAL DISTRIBUTION OF GALAXIES IN THE VIRGO CLUSTER

TYPE	No.	*e*-FOLD SCALE LENGTHS	
		Degrees	Mpc
E	30	1.4 ± 0.3	0.53 ± 0.12
S0	45	2.9 ± 1.2	1.08 ± 0.45
S + I	141	3.0 ± 0.7	1.12 ± 0.26
S0 + S + I	156	3.1 ± 0.5	1.15 ± 0.20
All types	186	2.6 ± 0.4	0.97 ± 0.16

b) *Radial Distribution*

The situation with regard to the radial distribution of galaxies is more clear-cut. The surface densities of galaxies in 1° annuli are shown in Figure 16. Ellipticals are binned separately from spirals and irregulars (the radial distribution of lenticulars is not shown). The two separate cases can be fitted nicely by exponentials. The parameters of the fits are given in Table 6. The linear scale lengths received the deprojection correction $4/\pi$, on the assumption that the distributions are spherical. It is clear that the ellipticals are more tightly confined to the center of the cluster than the other types, as was common knowledge. The characteristic scale length of the lenticular

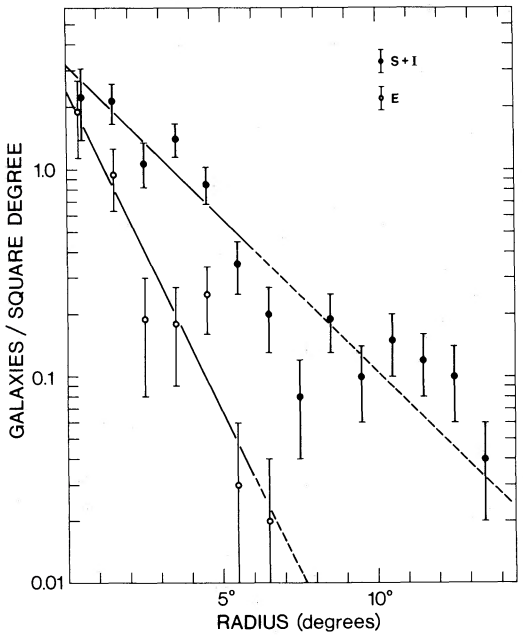

FIG. 16*a*

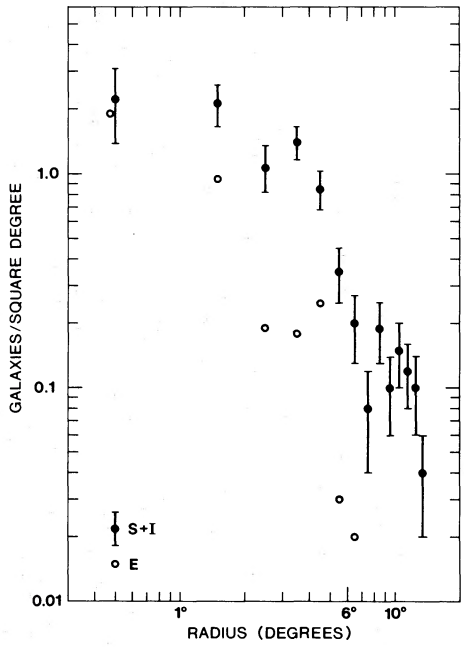

FIG. 16*b*

FIG. 16.—(*a*) Surface density of galaxies as a function of radius in the Virgo Cluster. (*b*) Surface density of galaxies as a function of log radius.

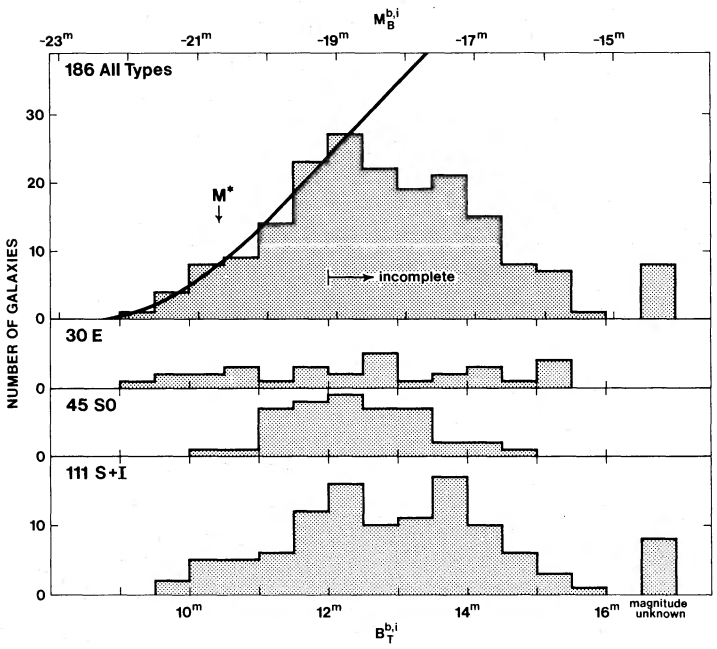

FIG. 17.—Luminosity function of galaxies in the Virgo Cluster. The solid curve illustrates the fit by a Schechter function.

distribution is similar to that for the spirals, but the uncertainty is large.

The point of Figure 16*b* is to emphasize that the exponential distribution implies a cutoff to the distribution on roughly the 6° scale of the cluster. If mass is distributed roughly like the galaxies, then this evidence is some support for a point-mass model since all the infalling galaxies lie outside this cutoff.

It can be seen already in Figure 2 but is found more dramatically in the deeper Center for Astrophysics redshift survey (Huchra, private communication) that there is spatial structure in the Virgo Cluster with internal velocity dispersions which are modest compared with the global cluster value. An example is the concentration of galaxies near SGL = 107°, SGB = −4°, which is seen in Figure 2*b* but not in Figures 2*a* or 2*c*.

c) *Luminosity Function*

The luminosity function of galaxies in the Virgo Cluster has been discussed by Kraan-Korteweg (1981), and we find ourselves in good agreement. The luminosity functions of three separate subgroups of our Virgo sample, and the ensemble, are all shown in Figure 17. As anticipated, incompletion sets in fainter than $B_T^{b,i} \approx 12.0$–12.5, roughly the Shapley-Ames limit after absorption corrections have been applied (Sandage and Tammann 1981). A Schechter (1976) function was fitted to the ensemble of galaxies with $B_T^{b,i} < 12.0$. The Schechter parameter α, which describes the slope of the faint end of the luminosity function, could not be tested by our sample because of incompletion and was set to the standard value of $\alpha = -1.25$. The best value for the Schechter parameter M^*, which defines a high-luminosity cutoff, was found by least squares fit to be $M^* = -20.70$. The Schechter function provides a good representation of the observed luminosity function at levels brighter than $B_T^{b,i} \approx 12.5$. It must be cautioned, though, that the coefficient α is badly constrained, and because there is a coupling between the parameters α and M^*, it means that M^* is also poorly determined. Fortunately the integrated luminosity is known to higher accuracy. Sandage (1982) has proposed that $\alpha = -1.5$ for ellipticals in the Virgo Cluster. Using this value for the ensemble leads to $M^* \approx -21.15$, but the integrated luminosity of the cluster is increased by only 18%.

The observed integrated luminosity to 12.0 mag in our sample amounts to $1.16 \times 10^{12}\ L_\odot$. The luminosity function with $\alpha = -1.25$ predicts that these galaxies contain 68% of the light in the cluster, so the total blue luminosity of the Virgo

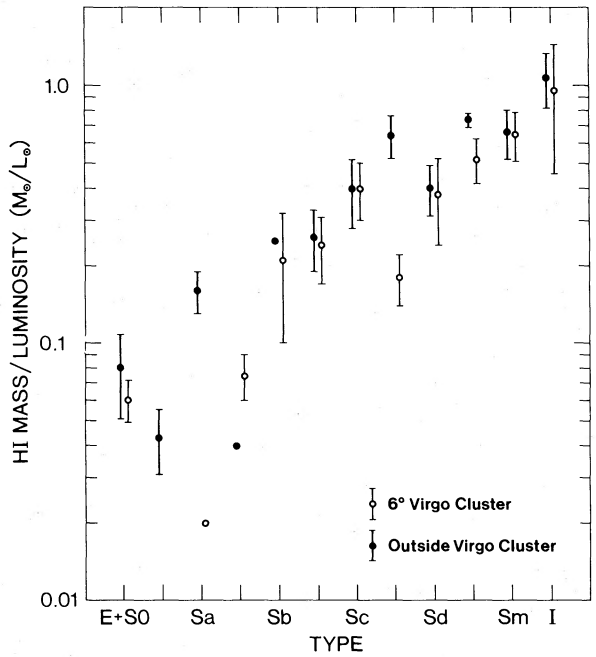

FIG. 18.—A comparison of H I mass-to-light ratios for Virgo Cluster spirals and spirals in the field.

Cluster would be $1.7 \pm 0.2 \times 10^{12}$ $L_\odot$. The observed luminosity in the 186 cluster galaxies in our sample is 1.48×10^{12} $L_\odot$.

d) H I *Deficiency*

It has become rather accepted that the spirals in the Virgo Cluster are deficient in H I by about a factor of 2 (cf. Chamaraux, Balkowski, and Gérard 1980; Giovanardi *et al.* 1983). Consequently, we were surprised, when we plotted Figure 18, by the lack of a significant difference between the H I properties of 50 galaxies inside the 6° Virgo Cluster and those of 50 galaxies outside. The systems involved in this analysis represent all the neutral hydrogen detections in the sample of 286 galaxies with $92 \leq \mathrm{SGL} \leq 117$, $-11 \leq \mathrm{SGB} \leq 8$ (see § II*a*). The galaxies contained by the "in" and "out" samples are at comparable distances in the mean and photometric information is of similar quality in the two cases.

Our analysis fails to confirm that there are significant differences in the H I content of Virgo spirals compared with spirals in less crowded regions. There is a substantial overlap between our sample and the one accumulated by Chamaraux, Balkowski, and Gérard (1980), and we find good agreement between us on the M_H/L values of individual galaxies. Most likely, the contradictory result that we get is due to differences in the control samples. Our control sample contains a large contribution from the infalling cloud in Virgo II. We would say that spiral galaxies which have already fallen into the Virgo Cluster do not have a significant H I deficiency compared with spirals which are now falling in. If the Virgo galaxies are truly H I deficient, then the infalling galaxies must also be somewhat deficient.

It is becoming apparent that spiral galaxies in many clusters *can* have normal H I content (Bothun, Schommer, and Sullivan 1982). There are questions regarding the H I deficiency in the Virgo Cluster which remain to be resolved, but they are not of great importance for the present discussion. We only note that there appear to be *both* gas-deficient spirals and spirals with normal H I content in the cluster environment. There are four cluster galaxies in our sample identified by van den Bergh (1976) as anemic, and all are H I deficient by factors of 2 or 3.

APPENDIX B

ARE SOME LOW-VELOCITY GALAXIES IN THE FOREGROUND?

We would just as soon have ignored the whole matter, but there are voices claiming that at least some of the galaxies that are the most blueshifted with respect to the Virgo systemic velocity are actually well to the foreground of the cluster. Holmberg (1961), Sulentic (1977), and McClure, Cowley, and Crampton (1980) have all argued in this fashion.

Recently, de Vaucouleurs (1982) has proposed that spirals occupy four zones in the line of sight toward Virgo, with inner shells in contraction and outer shells in expansion. In our opinion, only the proposition that some of the most blueshifted galaxies might be significantly closer than the mean Virgo distance begins to look convincing in the light of the observations. In fact, if only NGC 4569 is rejected from de Vaucouleurs's sample, then *none* of the bins identified *a posteriori* by de Vaucouleurs is at a distance which deviates by more than 2 σ from the cluster mean.

De Vaucouleurs (1982) specifically proposed that galaxies with $V_0 < 500$ km s^{-1} are associated with the foreground expanding region. We have searched the literature for information on the distances of Virgo galaxies with such low velocities. These galaxies are identified in Table 7. In each case that a distance was determined, we have evaluated whether it is compatible with the Virgo distance favored by the author of the distance, or to the foreground. If determined to be at the distance of the cluster, a V was entered into Table 7. If the measured distance was less than the Virgo distance by an amount that was considered to have a 3 σ significance, then an f was entered. If a galaxy appeared to be to the foreground but the significance was only ~ 2 σ, then an f? was entered. No case was ever made that any galaxy with $V_0 < 500$ km s^{-1} is behind the cluster.

Two conclusions are drawn, based on the information in Table 7: (i) There is rather conclusive evidence that NGC 4569 is to the foreground, and (ii) the evidence is not compelling that any other low-velocity system is to the foreground. The distance to NGC 4569 has been determined by a diverse set of independent methods: three variations of a color-magnitude relationship (Visvanathan and Griersmith 1977; Visvanathan and Sandage 1977; this paper), two variations of the magnitude–H I profile width technique (Helou, Salpeter, and Krumm 1979; Mould, Aaronson, and Huchra 1980), and a correlation between nuclear magnitudes and absorption band strengths (Cowley, Crampton, and McClure 1982). There is agreement that NGC 4569 is at about *half* the mean cluster distance. By contrast, there is no agreement that any other galaxy in Table 7 is to the foreground. Cases such as NGC 4192 and NGC 4413 warrant further consideration.

This discussion of the number of galaxies that reside to the foreground may seem to give a disproportionate emphasis to a minor matter, but it is actually quite important. We accept that whether or not a specific low-velocity galaxy is at the cluster distance, it is still *dynamically associated* with the cluster. The improbability of finding a blueshifted galaxy superposed by chance on the cluster has been pointed out by Sandage and Tammann (1976); anyway, none of the systems in question are so nearby that their systemic velocity could be in accordance with the Hubble expansion. It was seen in Figure 2*a* how well the low-velocity systems are concentrated toward the center of the cluster. Our model would allow that there could be blueshifted galaxies on the *far* side of Virgo just now falling in, but these are not observed. Galaxies that fell in some time ago would have passed through the cluster to the front side and still retain negative velocities. However, if there were a significant number of systems with extreme blueshifts at 3–5 cluster radii to the foreground, such a circumstance would represent a severe complication to our model.

Fortunately for us, there seems to be only one anomalous galaxy: NGC 4569. The SABab system NGC 4569 = M90 = Arp 76 would be one of the largest galaxies in the Virgo Cluster if it were at the mean cluster distance, but, taken to be at half the distance, it is unimposing. An exceptional case can be explained in terms of the gravitational slingshot mechanism (Saslaw, Valtonen, and Aarseth 1974) or as the tidal debris of a coalescence of two major cluster subunits. The former

TABLE 7

DISTANCES OF GALAXIES WITH $V_0 < 500$ km s^{-1} IN THE LINE OF SIGHT OF THE 6° VIRGO CLUSTER

Name	T	V_0	VG	VS	HSK	MAH	dV	CCM	This Paper
N4178	Sdm	285	...	...	...	V	f?	...	V
N4192	Sab	−220	...	...	V	V	f?	V	f
N4212	Sbc	−163	...	...	...	...	V	V	...
N4216	Sb	55	...	...	V	V	V	V	V
N4294	Scd	265	...	...	...	V	V	...	V
N4299	Sd	140	...	...	...	...	V	...	...
N4387	E	432	...	V	...	...	...	...	...
N4406	E	−419	...	V	...	...	...	f?	...
N4413	Sc	13	f	...	V	...	f?	...	...
N4419	Sa	−342	...	...	V	...	...	V	...
N4438	S0/a	165	V	...	f?	...	...	f?	...
N4442	S0	489	...	V	...	...	...	...	...
N4458	E	308	...	V	...	...	...	...	...
N4526	S0	354	...	V	...	...	...	V	...
N4548	Sb	406	...	...	...	...	f?	V	...
N4550	S0	302	...	V	...	...	...	...	...
N4552	E	159	...	V	...	...	...	...	...
N4569	Sab	−380	f	...	f	f	f	f	f
N4571	Scd	282	...	...	...	V	...	...	...
N4621	E	340	...	V	...	...	...	...	...

NOTES.—V, at distance of Virgo Cluster; f, foreground, $>3\ \sigma$ significance; f?, possible foreground, $\sim 2\ \sigma$ significance; VG = Visvanathan and Griersmith 1977; VS = Visvanathan and Sandage 1977; HSK = Helou, Salpeter, and Krumm 1979; MAH = Mould, Aaronson, and Huchra 1980; dV = de Vaucouleurs 1982; CCM = Cowley, Crampton, and McClure 1982.

mechanism is less attractive because the galaxy would have had to pass very near to other systems to have acquired an initial velocity of 3–4 times the cluster dispersion (say, within 10 kpc of a $10^{13}\ M_\odot$ object!), and it might be expected that the consequences would be noticeable. It is true that NGC 4569 is one of van den Bergh's (1976) anemic cases (Ab-c I–II), and it is somewhat deficient in H I. If it is now roughly 8 Mpc in front of the cluster, it has had 4×10^9 years to recover from the trauma.

Saslaw (private communication) proposed that the galaxy could have escaped with less wear and tear if it happened to have a large peculiar velocity and found itself outside the Roche limit of its parent subunit when a second major subunit came close. It could have been possible for the galaxy to drift outward to a distance comparable to the separation between the subunits without appreciable loss of kinetic energy. However since even today NGC 4569 retains a $2\ \sigma_V$ radial velocity component, the "subunits" in question *both* had to be comparable in total mass with that of today's cluster as a whole. The implication would be that the Virgo Cluster is the result of a merger between two comparably sized clusters which occurred roughly 4×10^9 years ago.

APPENDIX C

A VIRIAL ANALYSIS OF THE VIRGO CLUSTER

In view of our conclusion that perhaps all of the spirals in the Virgo Cluster are recent arrivals, an application of the virial theorem to this ensemble may seem reckless. The time scale for two-body relaxation in the cluster is long compared with the age of the universe, and the spiral newcomers would not have participated in the violent relaxation process that would have virialized the first generation members. The ellipticals may be relaxed, but they do not explore the full potential well of today's cluster. In sum, it might be feared that if the sample includes new arrivals with high velocities, then the virial mass will be overestimated, while a sample of only early systems would lead to an underestimate of the total cluster mass. These fears may be justified, but it turns out that two extreme cases lead to quite compatible results, and the indication is that the total mass of the cluster is, in fact, well constrained. In other respects, the situation favors an application of the virial theorem. The sample is large, and there are no serious problems with contamination, especially at the extrema in velocities.

The virial analysis was carried out on three samples: (*a*) all 186 galaxies with known velocities in the Virgo Cluster, (*b*) the 75 ellipticals and S0 galaxies in the cluster, and (*c*) just the 30 ellipticals. The detailed procedure of the analysis were described by Materne (1974) and Rood and Dickel (1976). The total potential energy of the cluster is computed by summing over the potentials between all possible pairs. The assumption is made that the mass in the cluster is distributed roughly like the galaxies. Corrections have been applied for measurement errors in velocities, following the prescription given by Materne, although in the case of the Virgo Cluster the velocity dispersion is so large that the adjustments are negligible.

With each of the three samples, two cases were considered. In one case, the virial analysis involved the standard mass weights, with the assumption of a constant mass-to-light ratio. In the second case, all galaxies were given equal weight.

There are several reasons for interest in the second case. If two-body relaxation processes have not been important, then there should be no tendency toward energy equipartition, and galaxies are expected to have similar kinematic and distributional characteristics in all mass intervals. In the mass-

TABLE 8

VIRIAL ANALYSIS OF THE VIRGO CLUSTER

Case	N_{char}	R_Ω (Mpc)	σ_V^* (km s^{-1})	M_{VT} ($M_\odot$)	t_c (years)
All types:					
1. Luminosity weights.....	18	0.77	750	9.6×10^{14}	...
2. Equal weights.....	186	0.76	716	8.6×10^{14}	3.6×10^9
E + S0:					
1. Luminosity weights.....	9	0.67	552	4.7×10^{14}	...
2. Equal weights.....	75	0.63	597	5.0×10^{14}	3.6×10^9
E only:					
1. Luminosity weights.....	5	0.49	590	4.1×10^{14}	...
2. Equal weights.....	30	0.42	678	4.3×10^{14}	2.1×10^9

NOTE.—Velocity dispersions are with respect to the mean velocity of the subsample. The virial radius is not adjusted for projection effects.

weighted virial analysis, relatively few galaxies play a dominant role, and there is little enhanced accuracy in extending the sample through the inclusion of large numbers of low mass systems. If only a few galaxies dominate the analysis, there are significant uncertainties due to projection effects and small number statistics. Bahcall and Tremaine (1981) have addressed these matters in connection with the slightly modified problem of groups dominated by a single massive member.

Results for the three samples and each case are summarized in Table 8. The parameter N_{char} is the measure of the number of galaxies effectively contributing to the analysis which was introduced in Table 4. The points made above are reinforced. In the luminosity-weighted cases, N_{char} are small compared to the total sample sizes. If there were equipartition, the velocity dispersions would be greater in the equal-weight cases, but there is no evidence of such an effect.

The results in each case are comparable, but we give preference to the equal-weight results. The total sample probably contains a substantial fraction of recent arrivals carrying inordinately large amounts of kinetic energy, which would cause an overestimate of the virial mass. The elliptical systems may be relaxed, but they do not occupy the full cluster potential well, so the solution based only on ellipticals must provide an underestimate of the total cluster mass. Our best estimate for the mass of the cluster is a compromise between these extreme limits:

$$M_{VIR} = 7.5 \pm 1.5 \times 10^{14}\, M_\odot .$$

An integrated blue luminosity of $1.7 \pm 0.2 \times 10^{12}\ L_\odot$ was determined for the cluster, so the mass-to-light ratio can be calculated:

$$M_{VIR}/L_B = 440 \pm 100\, M_\odot/L_\odot .$$

This result is in excellent agreement with both the early virial theorem calculations (Smith 1936; Oort 1958: $M_{VIR} \approx 7.5 \times 10^{14}\, M_\odot$) and the dynamical modeling by Hoffman, Olson, and Salpeter (1980: $M_{IF} = 6.7 \times 10^{14}\, M_\odot$).

The epoch of the initial collapse of the cluster, t_c, can be calculated following Gunn and Gott (1972):

$$t_c = 1.6 \times 10^{10} (R_\Omega^3/M_{14})^{1/2} \text{ yr}$$

where R_Ω, in Mpc, and $M_{14} = M_{VT} \times 10^{-14}\ M_\odot$ are parameters found in Table 8. There is a factor of 2 agreement in the value of t_c among the various samples. If only the ellipticals participated in the initial collapse, the moment of that event was when the universe was 2 billion years old, at a look-back redshift of 2.4 if the universe is closed.

REFERENCES

Aaronson, M., Huchra, J. P., and Mould, J. R. 1979, *Ap. J.*, **229**, 1.
Aaronson, M., Huchra, J. P., Mould, J. R., Schechter, P. L., and Tully, R. B. 1982, *Ap. J.*, **258**, 64.
Audouze, J. 1980, in *Cosmologie Physique*, ed. R. Balian, J. Audouze, and D. N. Schramm (Amsterdam: North-Holland), p. 195.
Bahcall, J. N., and Tremaine, S. 1981, *Ap. J.*, **244**, 805.
Bothun, G. D., Schommer, R. A., and Sullivan, W. T. 1982, *A.J.*, **87**, 731.
Capelato, H. V., Gerbal, D., Mathez, G., Mazure, A., and Salvador-Solé, E. 1982, *Ap. J.*, **252**, 433.
Chamaraux, P., Balkowski, C., and Gérard, E. 1980, *Astr. Ap.*, **83**, 38.
Cowley, A. P., Crampton, D., and McClure, R. D. 1982, *Ap. J.*, **263**, 1.
Davis, M., Tonry, J., Huchra, J. P., and Latham, D. W. 1980, *Ap. J.* (*Letters*), **238**, L113.
Davies, R. D., and Lewis, B. M. 1973, *M.N.R.A.S.*, **165**, 231.
de Vaucouleurs, G. 1958, *A.J.*, **63**, 253.
———. 1961, *Ap. J. Suppl.*, **6**, 218.
———. 1972, in *IAU Symposium 44, External Galaxies and Quasi-Stellar Objects*, ed. D. S. Evans (Dordrecht: Reidel), p. 353.
———. 1975, in *Stars and Stellar Systems*, Vol. **9**, ed. A. and M. Sandage and J. Kristian (Chicago: University of Chicago Press), p. 557.
———. 1982, *Ap. J.*, **253**, 520.
de Vaucouleurs, G., and de Vaucouleurs, A. 1973, *Astr. Ap.*, **28**, 109.
de Vaucouleurs, G., de Vaucouleurs, A., and Corwin, H. G., Jr. 1976, *Second Reference Catalogue of Bright Galaxies* (Austin: University of Texas Press).
Dressler, A. 1980, *Ap. J.*, **236**, 351.
Eastwood, T. S., and Abell, G. O. 1978, *Pub. A.S.P.*, **90**, 367.
Efstathiou, G., and Jones, B. J. T. 1979, *M.N.R.A.S.*, **186**, 133.
Fisher, J. R., and Tully, R. B. 1981, *Ap. J. Suppl.*, **47**, 139.
Giovanardi, C., Helou, G., Salpeter, E. E., and Krumm, N. 1983, *Ap. J.*, **267**, 35.
Gunn, J. E., and Gott, J. R. 1972, *Ap. J.*, **176**, 1.
Hainebach, K. L., and Schramm, D. N. 1976, *Ap. J.* (*Letters*), **207**, L79.
Helou, G., and Salpeter, E. E. 1982, *Ap. J.*, **252**, 75.
Helou, G., Salpeter, E. E., and Krumm, N. 1979, *Ap. J.* (*Letters*), **228**, L1.
Hoffman, G. L., Olson, D. W., and Salpeter, E. E. 1980, *Ap. J.*, **242**, 861.
Hoffman, G. L., and Salpeter, E. E. 1982, *Ap. J.*, **263**, 485.
Holmberg, E. 1961, *A.J.*, **66**, 620.
Hoyle, F. 1949, in *Problems of Cosmical Aerodynamics* (International Union of Theoretical and Applied Mathematics and International Astronomical Union), p. 195.
Janes, K., and Demarque, P. 1983, *Ap. J.*, **264**, 206.
Kraan-Korteweg, R. C. 1981, *Astr. Ap.*, **104**, 280.
Krumm, N., and Salpeter, E. E. 1979, *Ap. J.*, **227**, 776.
Materne, J. 1974, *Astr. Ap.*, **33**, 451.
McClure, R. D., Cowley, A. P., and Crampton, D. 1980, *Ap. J.*, **236**, 112.
Mould, J. R., Aaronson, M., and Huchra, J. P. 1980, *Ap. J.*, **238**, 458.
Oort, J. H. 1958, in *La Structure et l'evolution de l'universe* (Solvay Conference) (Brussels: Stoops), p. 163.
Ostriker, J. P. 1980, *Comments Ap.*, **8**, 177.
Peebles, P. J. E. 1969, *Ap. J.*, **155**, 353.
———. 1976, *Ap. J.*, **205**, 318.
———. 1979, in *Cosmologie Physique*, ed. R. Balian, J. Audouze, and D. N. Schramm (Amsterdam: North-Holland), p. 213.
Peterson, S. D. 1979, *Ap. J. Suppl.*, **40**, 527.
Rood, H. J., and Dickel, J. R. 1976, *Ap. J.*, **205**, 346.

Sandage, A. 1978, *A.J.*, **83**, 904.
———. 1982, communication at the workshop on dwarf galaxies, Tucson.
Sandage, A., and Tammann, G. A. 1975, *Ap. J.*, **196**, 313.
———. 1976, *Ap. J.* (*Letters*), **207**, L1.
———. 1981, *A Revised Shapley-Ames Catalog of Galaxies* (Washington: Carnegie Institution).
Saslaw, W. C., Valtonen, M. J., and Aarseth, S. J. 1974, *Ap. J.*, **190**, 253.
Schechter, P. L. 1976, *Ap. J.*, **203**, 297.
Shaya, E. J., and Tully, R. B. 1984, *Ap. J.*, **281**, 56.
Silk, J. 1974, *Ap. J.*, **193**, 525.
Smith, S. 1936, *Ap. J.*, **83**, 23.
Sulentic, J. W. 1977, *Ap. J.* (*Letters*), **211**, L59.
———. 1980, *Ap. J.*, **241**, 67.
Tammann, G. A. 1972, *Astr. Ap.*, **21**, 355.
Thuan, T. X., and Gott, J. R., III. 1977, *Ap. J.*, **216**, 194.
Tonry, J. M., and Davis, M. 1981, *Ap. J.*, **246**, 680.
Tully, R. B. 1982, *Ap. J.*, **257**, 389.
Tully, R. B., and Fisher, J. R. 1977, *Astr. Ap.*, **54**, 661.
———. 1984, *Atlas and Catalog of Nearby Galaxies*, in preparation (NBG).
Tully, R. B., Mould, J. R., and Aaronson, M. 1982, *Ap. J.*, **257**, 527.
van den Bergh, S. 1976, *Ap. J.*, **206**, 883.
———. 1982, *Pub. A.S.P.*, **94**, 459.
Visvanathan, N., and Griersmith, D. 1977, *Astr. Ap.*, **59**, 317.
Visvanathan, N., and Sandage, A. 1977, *Ap. J.*, **216**, 214.
Yahil, A., Sandage, A., and Tammann, G. A. 1980, *Ap. J.*, **242**, 448.

E. J. SHAYA and R. BRENT TULLY: Institute for Astronomy, 2680 Woodlawn Drive, Honolulu, HI 96822